FACULDADE DE CIÊNCIAS E TECNOLOGIA
UNIVERSIDADE NOVA DE LISBOA
Departamento de Química

Dynamic and Interaction of Cytochrome c with Pf1 Virus

Por: Patrique Nelson Ramos Nunes

Dissertação apresentada na Faculdade de Ciências e Tecnologia da Universidade Nova de Lisboa para obtenção do grau de Mestre em BioOrgânica.

Orientador: Doutor Francisco Jorge Caldeira

Juri: Doutor João C. Lima, assistido por Franciso J. Caldeira e presidido por Pedro J. Abreu

Maio de 2011

Dynamic and Interaction of Cytochrome c with Pf1 Virus

Acknowledgments

Muito são aqueles a quem devo uma palavra de apreço e gratidão por todo o apoio, e principalmente pela sua constante presença durante a realização desta tese. No entanto, não posso deixar de referir algumas pessoas. Ao professor Jorge Caldeira, quero agradecer ter-me aceite desde logo para a realização do estágio no seu laboratório. Quero ainda agradecer o incentivo e apoio constante que me deu ao longo destes últimos tempos, a disponibilidade para discutir qualquer resultado experimental e a informação transmitida para por exemplo efectuar um cuidadoso planeamento de experiencias, e ainda toda a sua amizade.

To Professor Peter Eaton, I want to express my gratitude for receiving me in his lab and for all the enthusiasm and information transmitted me over the last year or so.

Ao Prof. Dr. Nuno Santos, Marco Domingos e seus colaboradores, quero agradecer as instalações e equipamentos disponibilizados assim como toda a ajuda e o muito que apreendi com eles em na área de espectrofotometria (DLS e Potencial Zeta mais precisamente). A Ana Teresa toda a ajuda prestadada para a realização deste trabalho.

Um muito obrigado ao grupo de NMR; Eurico Cabrita, Maria do rosário e em especial para o Aldino pelas respostas às inúmeras perguntas que me foram surgindo.

Aos meus colegas e por último quero agradecer á minha família e amigos o constante incentivo a sua constante presença, e o facto de nunca me terem deixado de apoiar durante esta caminhada.

Aos meus pais e irmãos

À Cristina

Resumo

Palavras-chave: Citocromo c; vírus Pf1; Complexo Estequiometrico; interacção electrostática; Força iónica, DOSY-NMR.

O Citocromo c é uma proteína positiva e a superfície do Pf1 virus é negativa formando fortes complexos electrostáticos. Quando o rácio crítico de concentrações entre o Citocromo c e o vírus Pf1 é atingido surge a formação espontânea do seu complexo, cerca de 1.700 moléculas de citocromo c para uma partícula de Pf1. O efeito da concentração de sais no complexo formado foi medido por dispersão dinâmica de luz, Com o aumento da concentração de sal monovalente o complexo desagrega.

A dissociação gradual do agregado permite a obtenção dos espectros de RMN do citocromo c. Dependendo da relação vírus/Citocromo c ou da força iónica é possível a partir de proteínas e vírus livre em solução mudar para estado de ligação transiente ou formar um complexo totalmente imobilizado. A análise da variação dos deslocamentos químicos durante a titulação de sal permitiu mapear as regiões mais afectadas do citocromo c junto do co-factor hemico oxidado, devido à ligação ao vírus Pf1.

Amostras desidratadas e em estado de líquido com citocromo c e Pf1 em diferentes proporções e pHs foram observadas por microscopia de força atómica.

Acima da concentração de sal crítica de dissociação do complexo observou-se a diminuição gradual do coeficiente de difusão do citocromo causado pelo maior teor de vírus Pf1 em solução –(RMN DOSY-PGSE). Concluímos que existe uma forte correlação eletrostática entre o vírus PF1 e o Citocromo c mesmo depois de dissociação do complexo.

Abstract

Keywords: Cytochrome c; Pf1 virus; Stoichiometry Complex; Electrostatic Interaction; Ionic Strength; NMR-DOSY.

Cytochrome c is a positive protein and the Pf1 virus surface is negative forging strong electrostatic complex. When a critical ratio concentration of Cytochrome c and Pf1 virus is achieved a spontaneous complex is formed. The maximum association upon addition of cytochrome c to Pf1 solutions is about 1700 cytochrome c molecules to one Pf1 virion particle. The effect of univalent salt concentration on protein-polyelectrolyte complex formation was measured by Dynamic Light Scattering. Complex disaggregation occurred when monovalent salt concentration increased.

The assembly process was also observed by NMR at low salt concentration in the system. The aggregate can be gradually dissociated in order to enable NMR spectra acquisition. Depending on virus/cytochorme c ratio or ionic strength concentration we could shift from free protein and virus in solution to transient binding or fully immobilized complex. It was possible to map-the most affected regions of the oxidized heme cytochrome c, with chemical shift variation due to the binding to Pf1 virus, during salt titration.

Dry and liquid samples of Cytochrome c and Pf1 at different ratios and pH were studied and evaluated by Atomic Force Microscopy.

The system was also studied above the critical salt concentration of complex dissociation by PGSE-DOSY NMR. A gradual decrease in the translational diffusion coefficient of cytochrome was caused by higher content of Pf1 virus in solution. We conclude that a strong electrostatic correlation between pf1 virus and cytochrome c occurs even after complex dissociation.

Table of Figures

Table of Contents

Abbreviations and Symbols

Ø –diameter
l - Length
AcAm – Amonium Acetate
AFM - Atomic Force Microscopy
CNT - Carbon NanoTube
CPMV-Cowpea Mosaic Virus
Cyt c – Cytochrome c
D_{eff} – Effective Diameter
DLS - Dynamic Light Scattering
DOSY – Diffusion Ordered SectroscopY
EDL – Electrical Double Layer
EPR – Electronic Paramagnetic Ressonance
F-Actin – Actin filament
fd – Filamentous bacteriophage
HR-MAS - High Resolution Magic Angle Spinning
HRTEM - High-Resolution Transmission Electronic Microscopy
I. p. – Isoelectric Point
LbL - The Layer by Layer technique
LC – Liquid Crystal
M13 - The M13 Filamentous Virus
MT – Microtubules
NaCl – Sodium chloride
NMR – Nuclear Magnetic Ressonance
PALLES software to predict sterical molecular induction alignment.
PEG - Poly(Ethylene Glycol)
PEMs - PolyElectrolyte Multilayers
Pf1 – Pseudomonas phage Pf1
PGSE – Pulse Gradient -field Spin-Echo
RDC – Residual Dipolar Couplings
RNA & DNA – RiboNucleic Acid and DeoxyriboNucleic acid
SEM - Scanning Electron Microscope
Sm - Smectic phase
SMA - Shape Memory Alloy
SmA - Smectic A phase
SmC - Smectic C phase
STEM - Scanning Transmission Electron Microscope
TEM - Transmission Electron Microscopy
TMV – Tobacco Mosaic Vírus

1. INTRODUCTION

Nature provides inspiration for designing materials and systems that derive their functions from highly organized structures. In organisms, molecular recognition of metals by proteins control interactions and is following by the self-assembly to create major organization. Proteins could also be used in controlling materials formation in practical engineering via self-assembled, hybrid, functional materials structures. The matter manipulating on an atomic and molecular level means that all existent structure organization on nature can be called nanotechnology. Whether metallic for example Shape-Memory Alloys (SMA) are metals that, after being strained, at a certain temperature or electric field revert back to their original shape. A change in their crystal structure above their transformation temperature causes them to return to their original shape. SMA have applications in medical, and aerospace industries; whether organic like the fabrication of highly oriented carbon nanotube (CNT) on liquid-crystalline solution arrays to be used for thin-film transistors,[1] or even organo-metalics.

Over the past decades, self-assembly has attracted a lot of research attention and transformed the relations between chemistry, materials science and biology leading to self-assembly techniques. Three different research programs of self-assembly in nanotechnology in order to characterize their implications are: Hybridization (using the building blocks of living systems for making devices and machines; Biomimetics (making mimicking nature) and both of them used simultaneous[2,3]. Under certain conditions the molecules organize themselves into structures based on the principle of the weak interactions such as: hydrogen bridges; hydrophobic interactions; electrostatic and Van der Waals forces. There are a number of theoretical approaches on electrostatic binding, the most relevant effect is the counterion condensation theory expressed by the Poisson-Boltzmann equation[4]. The counterion distribution can be explained by a competition between thermal and electrostatic potential energy which regulate the counterion dissociation in the solution. The density charge of the ionic environment can be well described, considering the ion as a point charge at a distance (radius) in which like-charged objects such as polyelectrolytes electrostatic interactions between charged surfaces in water are dominated by counterion behavior.

On polyelectrolytes self-assembly even when electrostatic term appear to be the principal effect additional effects need to be take into account for organization material, such as steric; residues complementarity; excluded volume or ion size effect belonging to a short range interactions. The main difference between the long-range (electrostatic) and short range (specific) interactions is that the first strongly depend on the ionic strength while last one do not. The affinity of a counterion species for a polyion may be covalent, ionic, or non-ionic. Tight localized binding is also expected when the

nearest-neighborhood charge spacing on the polyion is sufficiently close, so that two or more groups can cooperate in holding the counterion. The larger the association constant, the larger will be both the number of associated counterions and the stability of each binding. Specific and nonspecific counterion binding occurs simultaneously while one can be the dominant.

One interesting material with unique properties of spontaneous self-assembly are the virus particles. Virus particles consist of a viral genome surrounded by a protein capsid. The genome can be single-stranded or double-stranded, composed of RNA or DNA, and stored in one or more polynucleotide chains. The surrounding capsid is assembled by the association of the repeat units of similar or identical proteins[5]. Experiments using genetic modifications of the M13 virus and synthesis of a heterobifunctional linker molecule were designed to specifically bind each modified virus end, leads to amazing 1D ring structure[6]. This genetic modifications set out to explore the possibility of encoding size and shape information into self-assembling other viruses. This kind of genetic modification provides a way to induce construction on a particular design or order. One end of the M13 virus was also genetically modified to nucleate or bind to a desired semiconductor material by A. Belcher group. These nanocrystal-functionalized viral building blocks were grown into ordered hybrid self-supporting films. In order to align other materials, anti-streptavidin viruses were the virus first selected to bind streptavidin protein units. This allows a universal handle for the virus to pick up any material that has been covalently conjugated to streptavidin. Then the self assembling nature of this anti-streptavidin virus can be exploited to make organized hybrid materials and the anti-streptavidin M13 viruses having specific binding for the streptavidin[7].

Genetic engineering also take advange of the protein repetitions to form the capsid virus, modifying substrate specificity of peptides to include some metals (ZnS, CdS; CoPt; FePt) for the synthesis of single-crystal, and chemically ordered nanowires. M13 has about 2700 copies of the gP8, which was genetically modified, and during nanoparticle nucleation peptides can been expressed on the highly ordered filamentous capsid of the M13 bacteriophage. The incorporation of specific, nucleotide peptides provides a viable template for the directed synthesis of semiconducting and magnetic materials or individual crystalline nanowires.[8]

With incorporations of ions in two building blocks of g8 protein genetic engeneering of M13 virus with Cobalt oxide and lithium, smaller and more flexible batteries can be developed. Incorporation of gold-binding peptides into the filament coat virus form a hybrid gold–cobalt oxide wires that improved battery capacity. Combining virus-templated synthesis at the peptide level controlling two-dimensional assembly of viruses on polyelectrolyte multilayers provides a systematic platform for integrating these nanomaterials to form thin and flexible lithium ion batteries[9].

1.1. Nanomaterials Fabrication Techniques

The Layer by Layer (LbL) technique is based upon the alternate adsorption of oppositely charged species from aqueous solution, and possesses unprecedented control of materials selection (e.g. polyelectrolytes, clays, nanoparticles, proteins), materials properties (e.g. conductivity, glass-transition temperature) and architecture (e.g. blends, stratified-layers, pores). These advantages make LbL assemblies excellent candidates for use in batteries, electrochromic devices, solar cells, sensors and drug delivery control. A. Belcher group worked on pharmacological drug delivery systems. These systems made possible to control the concentration to deliver the desired substances using LbL interfaces material. The same group use biological and non-biological assembly methods for fabricating and positioning small battery components that may enable high performance microbatteries with complex architectures[10]. Polyelectrolyte multilayers deposited by electrostatic LbL assembly techniques and others nanostructure electrodes or multidimensional architectures of new battery designs have an improvement on electrochemical performance. A self-assembled layer of virus-templated cobalt oxide nanowires serving as the active anode material in the battery anode was formed on top of microscale islands of polyelectrolyte multilayer´s serving as the battery electrolyte, and this assembly was stamped onto platinum microband current collectors. The resulting electrode arrays exhibit full electrochemical functionality. This versatile approach for fabricating and positioning electrodes may provide greater flexibility for implementing advanced battery designs and microelectrodes or 3D architectures. With an ever-increasing need for thin, flexible and functional materials in electrochemical systems, the LbL technique provides a simple and affordable route in creating new, active electrodes and electrolytes.

The same LbL technique was used to create a electrochemical systems device with thin, flexible multilayer which archive active electrodes and electrolytes for fuel cells based in proton-exchange membrane and direct methanol fuel-cells[9,11]. The electrostatic LbL assembly technique is an alternating deposition method between complementary charged species, which allows the creation of functional thin films and highly tunable surfaces through the control of electrostatic interactions. New methods are created based on self-assembly LbL technique employing the phenomenon of polymeric inter-duffusion, observed in some LbL assembled polyelectrolyte multilayers (PEMs). Competitive electrostatic binding between oppositely charged polyelectrolytes resulted in the segregation of virus molecules from the bulk of a multilayer film to the multilayer surface, yielding a two-dimensional ordered monolayer assembly of M13 viruses. The combination of electrostatic multilayer assembly and the virus monolayer provides a platform for the systematic integration of polymeric, biological, and inorganic materials. Direct assembly of M13 viruses on mobility-enhanced polyelectrolyte multilayer´s and achieve patterned LbL/virus assemblies on surfaces using a solvent-assisted capillary molding process[12]. Another way to produce new biomaterials is using the “bottom-up” approach. Materials are assembled molecule by molecule (is some cases even atom by atom) to make new

molecule architectures, requiring a deep understanding of individual molecular building blocks, their structures, assembly proprieties and dynamic behaviours. The chemical complementarities and the structural compatibility confer the weak and noncovalent interactions that bind building blocks during self-assembly[13]. Using the "bottom-up" method it is possible to prepare functional polymeric materials (semiconducting, metallic, and magnetic nanowires) based on self-assembly of polymeric supramolecules. The techniques constitute a general platform for constructing materials that combine several properties that can be tuned separately.

There are established ways to accomplish this by using various architectures of block copolymers, in which the structure formation is based on self-organization, that is, on the repulsion between the chemically connected blocks. Depending on the architecture, block length, and temperature, it is possible to obtain lamellar, cylindrical, spherical, or more complicated structures. This may be achieved by flow, by electric or magnetic fields, or by using topographically patterned surfaces. Molecules are constructed in order to recognize each other in a designed way. The subsequent supramolecules in turn form assemblies or self-organize, possibly even forming hierarchies. The overall alignment of the local structures can be additionally improved by electric or magnetic fields, by flow, or by patterned surfaces. The associations maintaining these and the associations of other cellular components seem relatively simple when examined by high-resolution structural methods (shape complementarity, charge neutralization, hydrogen bonding, and hydrophobic interactions). In contrast with the "bottom-up" there are the "top-down" approach, were the biomaterials are produced by slicing down a complex body into its component parts (for example, shave a virus particle down from its capsid to a viral cage)[14,15.] Another interesting way to make nanostructure is the idea that randomly arranged molecular species incorporated in a network medium can ultimately create ordered structures at the surface. Such order can be accommodated by regulating dynamic and equilibrium driving forces. M13 viruses ordered, highly complex biomacromolecules, driven by competitive electrostatic binding. The steric constraints inherent to the competitive charge binding between M13 viruses and two oppositely charged weak polyelectrolytes leads to interdiffusion and the virtual 'floating' of viruses to the surface. The result is a spontaneous formation of a two-dimensional monolayer structure of viruses upon a cohesive polyelectrolyte multilayer. This viral-assembled monolayer can be a biologically tunable platform to nucleate, grow and align nanoparticles or nanowires over multiple length scales. This system represents an interface that provides a general platform for the systematic incorporation and assembly of organic, biological and inorganic materials[16]. All these simples technique and possibility to create new complex and organized structures have attracted considerable attention due to their relevance for biological and therapeutic applications[17,18]. Filamentous biomaterials have been used as polyelectrolytes and have been important materials to study electrostatic effects on the lateral association. A number of filamentous biopolymers including actin filaments (F-actin), microtubules (MT), tobacco mosaic virus (TMV), and the filamentous bacteriophage fd form bundles under well-defined conditions. All of these

macromolecules are negatively charged, rodlike in shape, and lateral association is induced by a number of cations such as divalent and trivalent metal ions and homopolymers of basic peptides[19].

Wong and co-workers have used genetically engineered lysozyme with different monodisperse net charges to understand and manipulate the stability of self-assembled actin–lysozyme complexes (actin, an anionic polyelectrolyte, and lysozyme, a cationic globular protein). They discovered that in the presence of salt there was a high interaction between osmotic and electrostatic effects, showing that complexes between actin and lysozyme are stable with very high salt concentration. The existence of this counterintuitive like-charge attraction cannot be explained within the approaches such as the Poisson–Boltzmann theory. This fact is related to the osmotic pressure of the ion that is essential for the electrostatic bonds between particles of opposite charge. The changes in system energy translate thermodynamically in enthalpy changes. The explanation of the competition between thermal and electrostatic potential energy as a reason for counterion binding. For the stronger binding of multivalent ions onto polylelectrolytes the reason is not the stronger electrostatic force, but it is due to entropic effects which keep the free energy of this process negative (as it occurs spontaneously)[20,21].

Mixing solutions of polyanions and polycations leads to spontaneous aggregation under release of counterions. The level of aggregation depends on the nature of the components, on the medium and external conditions. For free polyelectrolyte chains the low molecular mass counterions are more or less localized near the macroions in the case of high charge densities, particularly because of counterion condensation. However, other interactions such as hydrogen bonding hydrophobic steric effect may play an additional part to order particles organization[22].

1.2. Molecular Assembly Models

Understanding the physical principles governing directed macromolecular assembly is problematic because the assembly in those systems is driven by strong ionic and covalent interactions and steric factors are of minimal importance. A model system chosen by De Yoreo et. Al was Cowpea Mosaic Virus (CPMV) genetically engineered to present histidine tags around the capsid apexes to bind specifically and reversibly at nanoscale chemical templates. They have shown that the physics of directed macromolecular assembly can be understood by combining principles governing small molecule with those that drive colloidal condensation in confined systems. Experiences with poly(ethylene glycol) (PEG) to induce the lateral expansion of virus clusters suggests a significant role for weak interactions[23]. There are innumerous programs that simulate the docking of molecules or proteins, Chemera/Bigger for instance take the crystallographic molecules structures and produce an algorithmic with some interaction, such as electrostatic, hydrophobic and residues complementary. Other brilliant program that simulates electrostatic interaction is based on Monte Carlo simulation. Essentially this mathematical method can calculate the osmotic pressure versus inter-rod separation for

ordered arrays of charged rods in equilibrium with a bulk salt solution corresponding. Alexander P. Lyubartsev have done calculations of the electrostatic osmotic pressure for a closely packed phase of laterally ordered rodlike fd or M13 virus particles at equilibrium with a bulk salt solution. This direct application of simulation to a specific experimental system is made possible by performing the Monte Carlo simulations within the grand canonical ensemble and the calculations agree with the results from light scattering measurements, salt titrations and NMR result in this work which sensitively detect the formation of laterally ordered virus aggregates,[24].

Self-organization of molecules can be obtained by applying an external field, such as electric, magnetic or mechanic. Self-assembly of two building blocks affinities is the beginning in order to create structures but is it has been demonstrated that several types of rod-shape viruses form well-controlled liquid-crystalline phases like tobacco mosaic virus or M13 virus. Fibers made from liquid crystalline suspensions with M13 virus solution just passing through a micrometer diameter capillary to a cross-linking solution resulting in a nematic ordered morphologies due to flowing forces with 10-20um diameter[25]. These nanocrystal-functionalized building blocks were grown into hybrid ordered self-supporting films. The resulting nanocrystal hybrid film was also ordered including the chiral effects of virus building blocks and providing strong evidence that virus-based film are organized into chiral scemetic C structures (see Fig. 1.1)[26].

1.3. Liquid Crystal

Liquid Crystal (LC) materials are a state of matter that share properties of the liquid and crystalline states of matter where molecules have no positional order (like a fluid), but point in a particular direction on average or molecules may form layers in one direction, like a crystal. A LC may flows like a liquid, but its molecules may be oriented like a crystal. The possibilities are nearly endless, with different arrangements of layers, columns, twists and turns coexisting with fluid movement.

The simplest and least-ordered phase of liquid crystals is the nematic phase (N) where rod-like molecules point on average in a particular direction called the director, **n**. (see Figure 1.1). The second common phase is the smectic phase (Sm), where the molecules form layers of thickness approximately one molecular length.

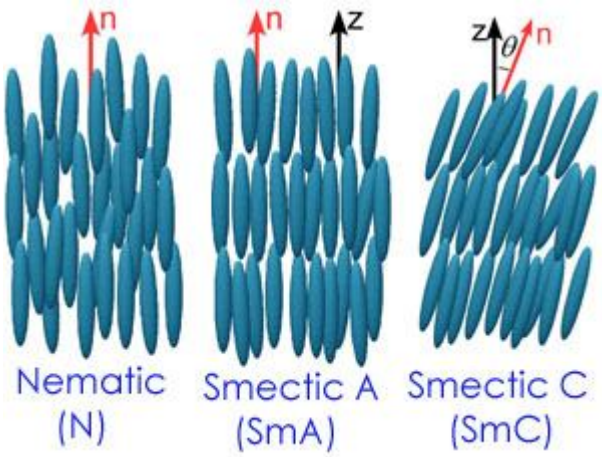

Figure 1.1: Ordered phases of a thermotropic liquid crystal arranged from left to right in order of increasing order and decreasing temperature[27].

We can define a direction perpendicular to the layers' plane, known as the layer normal, z. There are two basic smectic phases (although many more exist): the smectic A phase (SmA) where the director **n** points in the same direction as the layer normal, **z**; and the smectic C phase (SmC) where the director, **n**, points at some angle to the layer normal, **z.**

Materials may display one or more of these liquid crystal phases and in general the phases occur in the following order with decreasing temperature: isotropic liquid, nematic, smectic A, smectic C, crystal. Liquid crystals have very sensitive electrical and optical, or electro-optic, properties. It is possible, for example, to orient rod-like liquid crystal molecules by applying an electric field: the field induces a separation of charge in the molecules, producing a torque which tries to align the molecules with the direction of the field.

Functionalized liquid-crystalline materials using virus might provide various pathways to build well-ordered and well-controlled two and three-dimensional structures for the construction of next generation optical, magnetic materials and electronic devices. Even in the presence of multivalent cations, strongly charged anionic polyelectrolytes such as DNA and F-actin can assemble into densely packed aggregates with a behavior of a liquid crystal[28].

1.4. Magnetic field orientation

A liquid crystal system was also used for the fabrication of a highly ordered composite material from genetically engineered M13 bacteriophage and (ZnS) nanocrystals. The bacteriophage was coupled with ZnS solution that self-assemble and develop a self-supporting hybrid film material. The result was a highly oriented, self-supporting films. In addition viral suspensions were prepared in which the liquid crystalline phase behaviours of the hybrid material were controlled by solvent concentration and

by the use of an applied magnetic field. Many particles orientation was observed by Atomic Force Microscopy such as radial or paralleled geometries organization[29].

In solution molecules with an anisotropic magnetic susceptibility will align with the static magnetic field to an extent that is proportional to the magnitude of the susceptibility anisotropy and the square of the magnetic field strength. As a result, by NMR experiments, dipolar couplings have a residual, non-zero value, and chemical shifts depend on B_0. This means magnetic field dependent chemical shifts therefore are potentially quite useful as constraints in macromolecular structure determination. Experiences with protein backbone amide ^{15}N nuclei from a DNA fragment were carried with good correlation with the dipolar couplings and the field dependence of the ^{15}N shifts[30].

1.5. Pf1 -Bacteriophage

Filamentous bacteriophages have been used to fabricate interesting materials such as robust fibers thin films, genetically engineered to attached quantum dots to produce nanowires[31] for fuel cells[32]. Pf1 bacteriophage (Figure 1.2) has been intensively studied regarding their liquid crystal thermodynamic properties[33] derived from their peculiar rod shape[34] (l=2µm, ø=6,7 nm), virus capsid protein are strongly negatively charged (-0,472e-/nm2) (I. p. =4.0), due to the presence of 3 aspartic acid and no other charged residues[35.] Their semi rigid nature (persistent length 2,2µm)36 and molecular mass 37 MDa, monodispersity and 3D structure with high resolution[37].

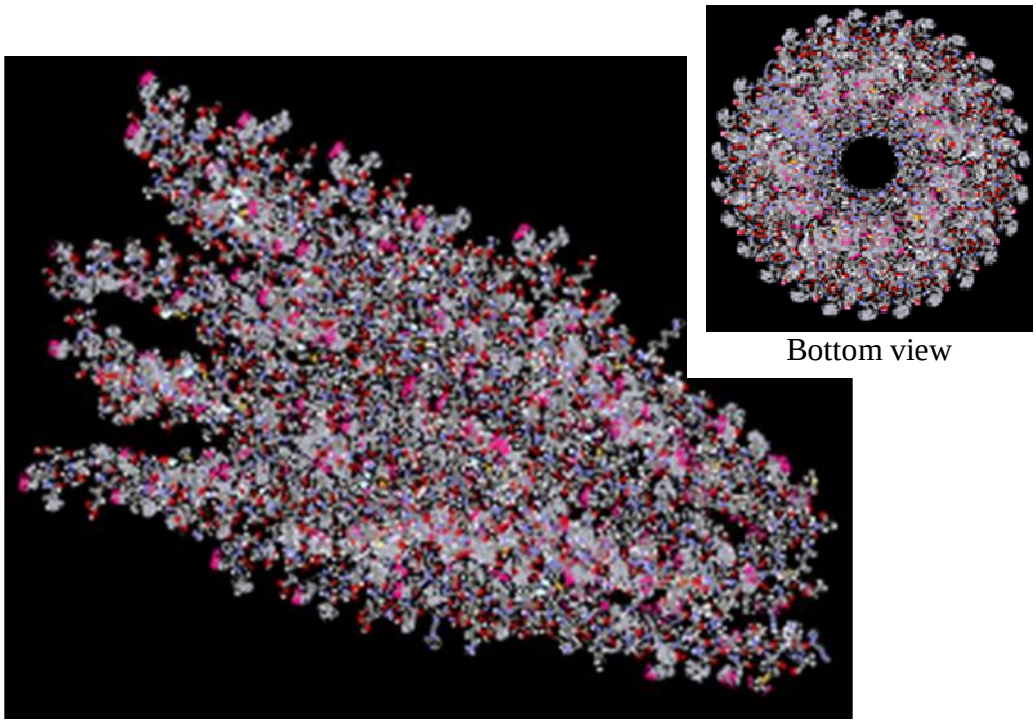

Figure 1.2 – Representation of Pf1 bacteriophage capsid structure models coloured. Sites mapping to the outer surface of the virion exposed to solvent. The views are of only a small section of the entire Pf1 virion[38].

Its tubular structure has ~4700 protein capsid subunits of 46 aminoacids in the outside with a single strand DNA inside (one subunit per DNA Base) plus some terminal proteins. Due to its high molecular mass Pf1 virus particles are not observable in liquid state NMR. When in the presence of a strong magnetic field[39] (>7 Tesla, NMR spectrometer range) the Pf1 virus have an order parameter S higher than 0.9, indicating that the rod virus particles are mostly aligned in a direction parallel to the applied magnetic field. This effect in caused by the sum of the magnetic anisotropy of each capsid protein subunit that is arranged along the virus axis. This liquid crystalline order is also favored at high concentration (>10-15 mg/ml) due to the reduction of exclude volume in solution[40]. However the strongly negative charged nature of the virus contraries the parallel packing since it maximize electrostatic repulsion, making the perpendicular arrangement of the virus the most favorable electrostatic arrangement.

The influence of the electrostatic field that causes virus-virus repulsion can be more easily pictured with the help of the effective diameter D_{eff} concept[41]. Since the electrostatic field is a dependent on pH and salt this experimental parameter are easy to control the magnitude of D_{eff} . The D_{eff} can range from (6,7nm) of the bare virus diameter (at high ionic strength or I.p. pH) to much larger (up to 60 nm) at low (~ 1mM) ionic strength[42] and neutral pH. The liquid crystalline properties of this solution are therefore critically controlled by these experimental parameters. Detailed theoretical and experimental study of their liquid crystalline properties regarding, pH, ionic strength, applied mechanic or magnetic field are described[43]. The virus spontaneously tendency to form fibers enabled the determination of their X-ray diffraction[44] and solid state NMR[45] three-dimensional derived structure. With the generalized application of residual dipolar couplings (RDC) in NMR[46] a great deal of research was done in order to find suitable aligning matrix for molecules in solution. Pf1 virus is one of the most versatile aligning media and their results can be predicted with PALES software[47].

It was early recognized that a tunable amount of weak alignment could be imposed to the free proteins in solution depending on experimental conditions. The imposed order parameter is weak (ranges around ~10-5 to 10-6) and adjusted for RDC determination. Higher alignment yields observed dipolar coupling too large increasing spectra complexity. The alignment of solute molecules in solution by a matrix is always dependent on the flexibility of the solute molecule their aspect ratio and charge distribution. Previously we have shown than a partially aligned array of D.gigas cytochrome c3 microcrystals can be aligned in a liquid crystalline Hydroxypropyl cellulose media. The resulting thin films display a great enhancement of sensitivity and resolution for EPR spectroscopy, and a spatial orientation distribution function of the molecules of the sample can be obtained[48].

1.6. Horse Heart Cytochrome c

Cytochrome c is a highly conserved protein across the spectrum of species, found in plants, animals, and many unicellular organisms in other words, every eukaryotic cell living on earth. This protein is associated with the electron transport chain inner membrane of the mitochondrion. Cytochrome c is a small size (molecular weight about 12,000 daltons) and highly soluble protein, unlike other cytochromes, with a solubility of about 100 g/L makes it useful in studies of cladistics. Its primary structure consists of a chain of about 100 amino acids. Many higher order organisms possess a chain of 104 amino acids[49].

It is known that cytochrome c is a soluble protein with a positively charged lysine rich region around the exposed heme edge that constitutes the binding domain based on electrostatic interactions with both reaction associates. However, proteins carry positive and negative charges on their surface depending on the functional groups present in the molecule and may be regarded as polyampholytes. Their behaviour in solutions of electrolyte as the function of the pH can be understood on this basis[50] The net charge on the protein is affected by pH of their surrounding environment and can have a net positive or negative charge which is balanced at the isoelectric point. As a result, proteins can interact with linear polyelectrolytes of opposite charge in solution.

Horse heart cytochrome c (Figure 1.3) is a well known studied protein with assigned functions electron transfer and apoptosis. It is capable of undergoing oxidation and reduction. It transfers electrons between Complexes III and IV. Remarkable spectroscopic properties of paramagnetic heam Fe (III) low spin oxidized state, induces large variations of chemical shifts in the groups in the vicinity of the metal center[51.] These shifted resonances are very sensitive to molecular interactions and therefore ideal to probe to study cytochrome c / protein capsid Pf1virus interactions. Small variations of the unpaired spin density in the heam causes by small conformational alteration producing large changes (few ppm) in the observable chemical shifts.

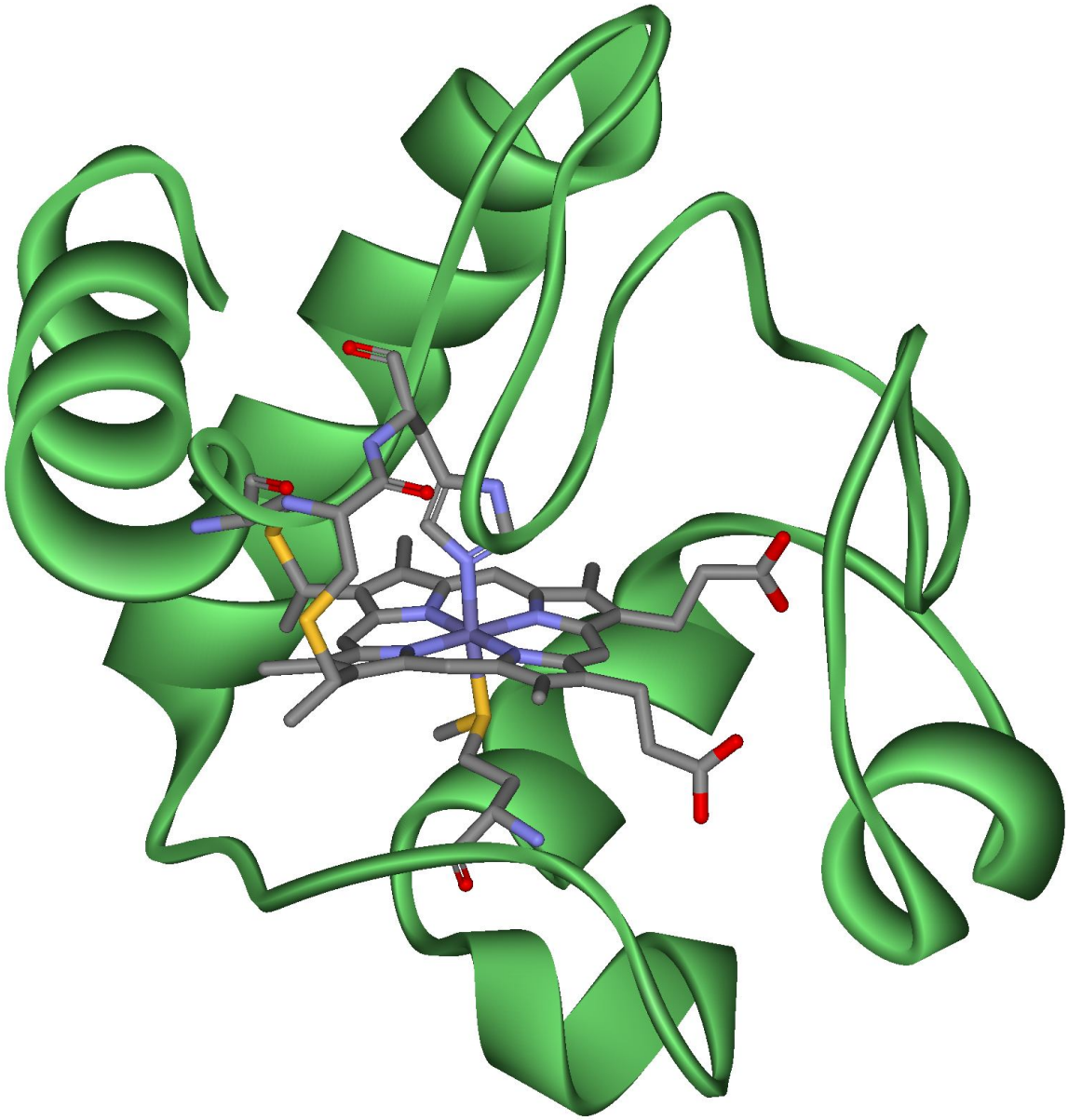

Figure 1.3 – Representation of horse heart cytochrome c structure (green- aminacid chain; in the center the Heme[52]

1.7. Analytic techniques

To study interactions of building blocks in solution or organized material, many techniques are currently being used, such as: synchrotron small-angle x-ray scattering; Electron microscopy (SEM; TEM; STEM; HRTEM); laser-scanning fluorescence microscopy; Solid-state NMR or at the magic angle (HRMAS); Crystallography etc. In this work we have used essentially five techniques: The traditional UV-Visible spectrometer; the topographic Atomic Force Microscopy (AFM) technique; Dynamic light scattering; Zeta Potencial and -DOSY- PGSE-1H-NMR. The following section just gives a brief equipment description.

1.7.1. Atomic Force Microscopy (AFM)

AFM is a technique that measures the three dimensional image of any solid surface of a sample using a sharpened probe, (Figure 1.4).

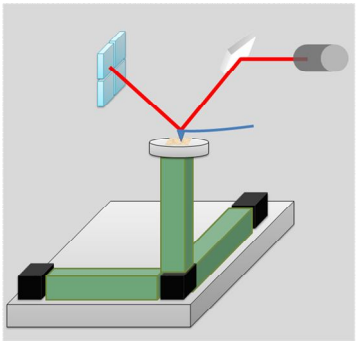

Figure 1.4 - Light Lever Sensors AFM Block diagram of the electronics employed for vibrating mode AFM scanning. The signal used for feedback can be selected phase or amplitude[53].

This instrument can measure images at atomic range.It is essentially composite by a computer, electronics control and a controlled sample position. The diagram on figure 1.4 illustrates a circuit with phase/amplitude detection in the AFM. A laser light is reflected of the back side of a cantilever into a 4 section photodetector. When the probe interacts with the surface the reflected light path will change. The force is then measured by monitoring the change in light entering the 4 quadrant photo-detector. Geometrically, the deflection at the end of the cantilever is equal to the motion of the laser beam across the face of the photo detector. In addition, mechanically modulate, or vibrate the cantilever is often to be a great advantageous to AFM, comparing the modulated signal phase or amplitude to the drive frequency. Summarizing there is several ways to convert electronic signals into images. These signals have different source of the same images: the voltage that goes to the Z piezoelectric ceramic, after the feedback controller; the output of the light lever photo-detector; the measures the displacement of the z ceramic and the amplitude and phase demodulator[54 55.]

Theretofore, dry samples were a requirement for this technique, but more recently liquid cells were developed consisting to put the sample and the tip (sample/probe) in an isolated liquid environment and scanning the particles that are on silica surface. Liquid cell bring enormous advantages since samples can be analyzed keeping the chemical interactions on the know solution conditions. In really, is possible to see the particle behaviour that are attached to the surface when interacting with the solution molecules.

1.7.2. Dynamic Light Scattering (DLS)

The advantage of the Dynamic Light Scattering to AFM technique is the possiblility to determine the size distribution of small particles in suspension or polymers in solution.[56]

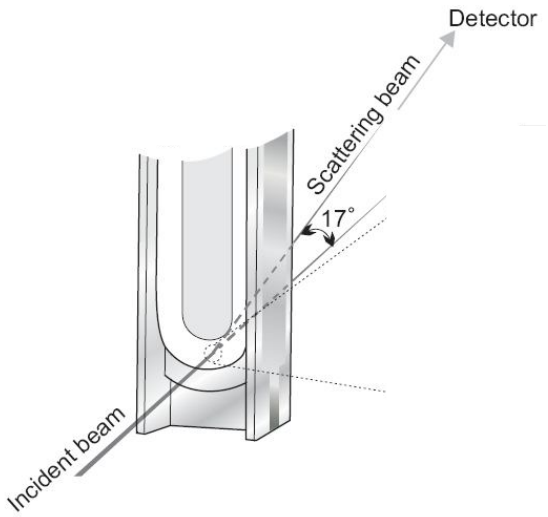

Figure 1.5 - The light scattered at an angle of determined angle is combined with the reference beam. This produces a fluctuating intensity signal where the rate of fluctuation is proportional to the speed of the particles. A digital signal processor is used to extract the characteristic frequencies in the scattered light.[57]

This instrument consist on analyze the light scatters that change in all directions (Rayleigh scattering) when a monochromatic laser light hits small moving particles. This change is related to the size of the particle. The light laser passes through a lens and then hits the cell with the solution. The light is scattered and detected by a photomultiplier that transform a variation of intensity into a variation of voltage (photoelectric effect).

The experiment's theory is based essentially on two assumptions. The first condition is that the particles are in Brownian motion, as in this situation we know the probability density function. The second assumption is that the beads used in the experiment, are spherical particles with a diameter equivalent to the molecular dimensions. If it is, then it is possible to apply the Stoke-Einstein relation and hence have a formula that easily gives the diffusion coefficient constant (see NMR DOSY section)[58.]

To fit the autocorrelation data have been generated (e. g. the autocorrelation function) numerical methods are used, based on calculations of assumed distributions, different mathematical approaches can be employed. Analysis of the scattering is facilitated when particles do not interact through collisions or electrostatic forces between ions. [59,60]

Depending on the anisotropy and polydispersity of the sample, a resulting plot may or may not show an angular dependence. Small spherical particles will show no angular dependence, hence no anisotropy. Particles with a shape other than a sphere (like a rod) will show anisotropy and thus an angular dependence. In most cases, samples are polydisperse. Thus, the autocorrelation function is a sum of the exponential decays corresponding to each of the species in the population. A few methods have been developed to extract as much useful information as possible from an autocorrelation

function available in software packages. One of the most common methods is the cumulative method (far less affected by experimental noise). The first order correlation function of laser light scattered by polydisperse solutions of macromolecules can be written as a sum or distribution of exponentials, with decay rates proportional to the diffusion coefficients of the solute molecules. It is shown that the logarithm of this correlation function is formally equivalent to a cumulant generating function[61].

1.7.3. Zeta Potential

Zeta potential is just a technique to obtain more information about the system using the same supporting DLS equipment. Zeta potential is based on dynamic light scattering, with the advantage of characterize "particles charges". Sized colloidal particles and biological macromolecules typically become charged due to; the dissociation of ionic groups at the particle surfaces into the solution; receive charge is by ion adsorption or by unequal dissolution of the oppositely charged ions of which the particles are composed.[62]

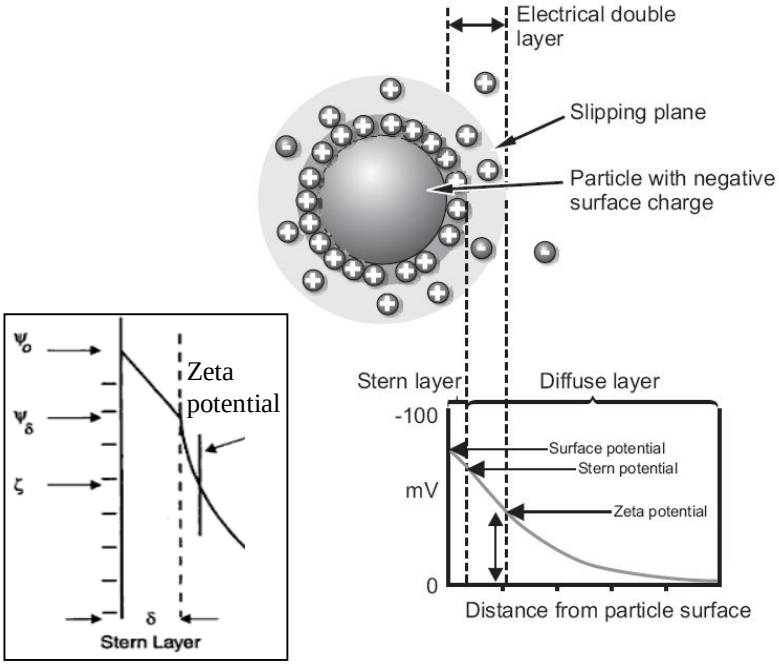

Figure 1.6 **a)** Right - Schematic of the electrical double layer and the line represent the electrical double layer distribution. The electrical potential distribution (ψ0; ψbulk) on the bulk solution can be described by the Poisson distribution by Gouy model.[63] **b)** Left – Zoom in of the potential distribution were: (ψ0) surface potential; (ψ) Stern potential and (ζ) Zeta potential

When a particle moves (ex.: due to an applied electrical field), ions within the boundary move with it, but any ions beyond the boundary do not travel with the particle. This boundary is called the surface of hydrodynamic shear or slipping plane. The potential that exists at this boundary is known as the zeta potential (Figure 1.6 b) that is possible to be calculated, using theoretical models or can be experimentally. From the instrumental viewpoint applying an electric field across the dispersion, particles within the dispersion with a zeta potential will migrate toward the electrode of opposite

charge with a velocity proportional to the magnitude of the zeta potential. The receiving optics is focused so as to relay the scattering of particles in the cell. The frequency shift or phase shift of an incident laser beam caused by these moving particles is measured as the particle mobility, and this mobility is converted to the zeta potential[60].

The values of the ζ-potential can give a great contribution to understand the dynamic of a particles aggregation system. If all the particles in suspension have a large negative or positive zeta potential then they will tend to repel each other and there is no tendency to flocculate. However, if the particles have low zeta potential values then there is no force to prevent the particles coming together and flocculating. i. e., attraction exceeds repulsion and the dispersion will break and flocculate. A value of 30 mV (positive or negative) can be taken as the arbitrary value that separates low-charged surfaces from highly-charged surfaces[64]. Summarizing zeta potential indicates the degree of repulsion between adjacent, similarly charged particles in dispersion. Zeta potential is particularly dependent of the pH and we can easily deduce the ζ-potential vs pH curve. (Positive at low pH and lower or negative at high pH).[65], [66], [67]

1.7.4. NMR - Diffusion Ordered SpectroscopY (DOSY)

Diffusion Ordered Spectroscopy is a non invasive or destructive technique that gives precious information about the dynamics of particles on solution. Simultaneously with the theory of molecular mobility this technique was developed and able to measuring diffusion coefficients or self-diffusion[68]. Similar to DLS this technique, it considers that the molecules motion have Brownian molecular motion and the diffusion behaviour is a measure of the translational motion of a molecule. It depends on several parameters like: size; shape of the molecule, as well as physical properties of the surrounding environment such as viscosity, temperature, etc. Assuming a spherical shape, size of the molecule the diffusion coefficient D is described by the stokes-Einstein equation

$$D = \frac{kT}{6\pi\eta r_s} \qquad \text{(eq. 1.1)}$$

Were k is the boltzman constant, T the absolute temperature, η the viscosity of the liquid and rs the hydrodynamic radius of the molecule. The study of self-diffusion by NMR can be performed by use of gradient field that can spatially labelled molecules, i.e. marked depending on their position in sample tube. As the gradient increase the diffusion signal intensity drop off, is attenuated depending on the diffusion time Δ and the gradient parameters (g, δ). This intensity change is described by:

$$I = I_0 \times e^{-D\gamma^2 g^2 \delta^2 \left(\Delta - \frac{\delta}{3}\right)} \Leftrightarrow \frac{I}{I_0} == \exp\left[-D \times q^{2\left(\Delta - \frac{\delta}{3}\right)}\right] \qquad \text{(eq.1.2)}$$

Where I is Intensity at the echo with gradients, I_0 Intensity at the echo without gradients, D Self-diffusion coefficient, γ the gyromagnetic ratio of the observed nucleus, g the gradient strength, δ the

length of gradient, and Δ the diffusion time.[69]. When a ^{1}H-NMR spectra is acquired each nuclear spin is identified by its larmor precession frequency (ω_0) which is dependent of the Magnetic field applied. By measuring nuclear spins special positions at two distinct time's information about their displacement. The first gradient field applied can spatially label the nuclear spins (coding) keeping the duration of gradient (δ) constant. After waiting the diffusion time (Δ) the second opposite gradient pulse is applied, to refocus the nuclear spins give to us some information about the quantity of spins that really are refocusing which means that the molecules that have moved on the diffusion time (Δ) are not in position to refocus their magnetization on the decoding phase. [70]

This technique is definitely a great progress as a way to separate different compounds in a mixture based on the differing translation diffusion coefficients of each chemical species in solution. In a certain way, it can be regarded as a special chromatographic method for physical component separation, but unlike those techniques, it does not require any particular sample preparation or chromatographic method optimization and maintains the innate chemical environment of the sample during analysis. (Figure 1.7).

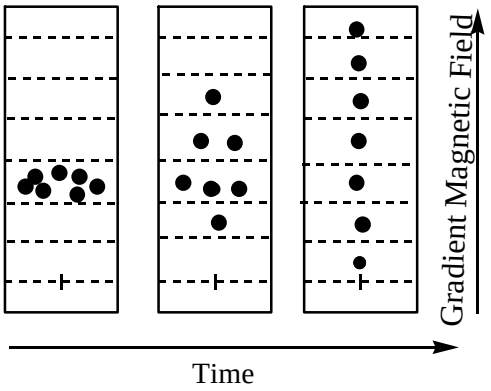

Figure 1.7 – Representation of labeled particles samples motion on a NMR tube applying a gradient of Magnetic field in function of time (diffusion time).

2. RESULTS

2.1. Complex stoichiometry of the Pf1/ Cyt c mass ratio

The results of the assay of complex formation in mixtures of cytochrome-c and Pf1 solutions are presented in Figure 2.1 where the dependency of the residual absorbance (free cytochrome c not involved in the precipitation) on the composition of the mixture is shown. Values of absorbance at 410nm were measured to account for cytochrome c concentration remained in solution after its aggregation with Pf1 virus and centrifugation of the pellet. As we can see, for 0.6mg/ml and 0.25mg/ml Pf1 concentrations, the highest aggregate formation appeared at 0.15mg/ml and 0.3mg/ml cytochrome c concentrations, respectively.

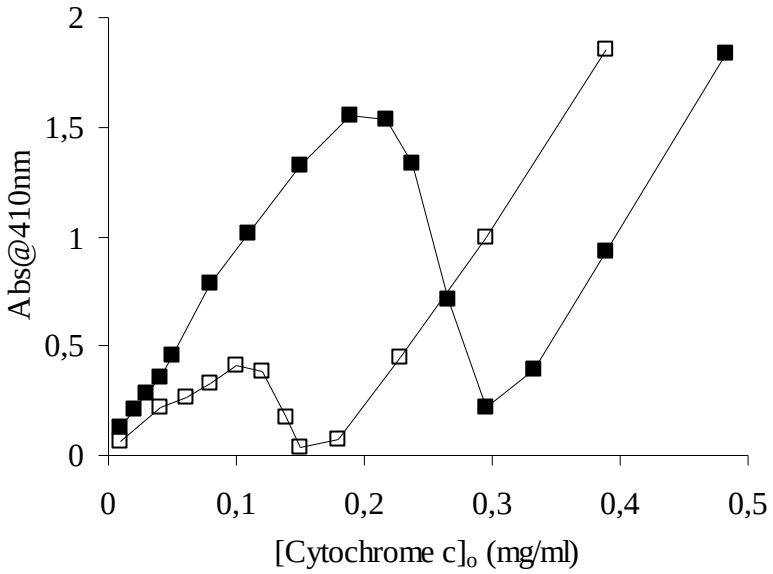

Figure 2.1 - Cytochrome c absorbance in the supernatant (after centrifugation of the precipitated complex) determined by UV-Visible spectroscopy at 410nm. Cytochrome c was stepwise added in order to have increasing cytochrome c concentration in the cuvette, with two Pf1 virus concentrations: (■) 0.25mg/ml and (□) 0.6mg/ml.

A mass balance for cytochrome c was used to calculate the amount of cytochrome c bonded to Pf1 virus. The results are displayed in Figure 2.2 a) for three titration curves, each region of sharp change in capacity value locates a critical condition in which cytochrome c ions condense to the Pf1 virus. At such condition, the attractive interaction due to cytochrome c has just reached a balance with the interfilament repulsion, and aggregates start to form. The cytochrome c concentration for the highest capacity value was determined according to the maximum value of Q (Fig. 2.2a) and plotted vs. the Pf1 molar concentration (Fig. 2.2b).

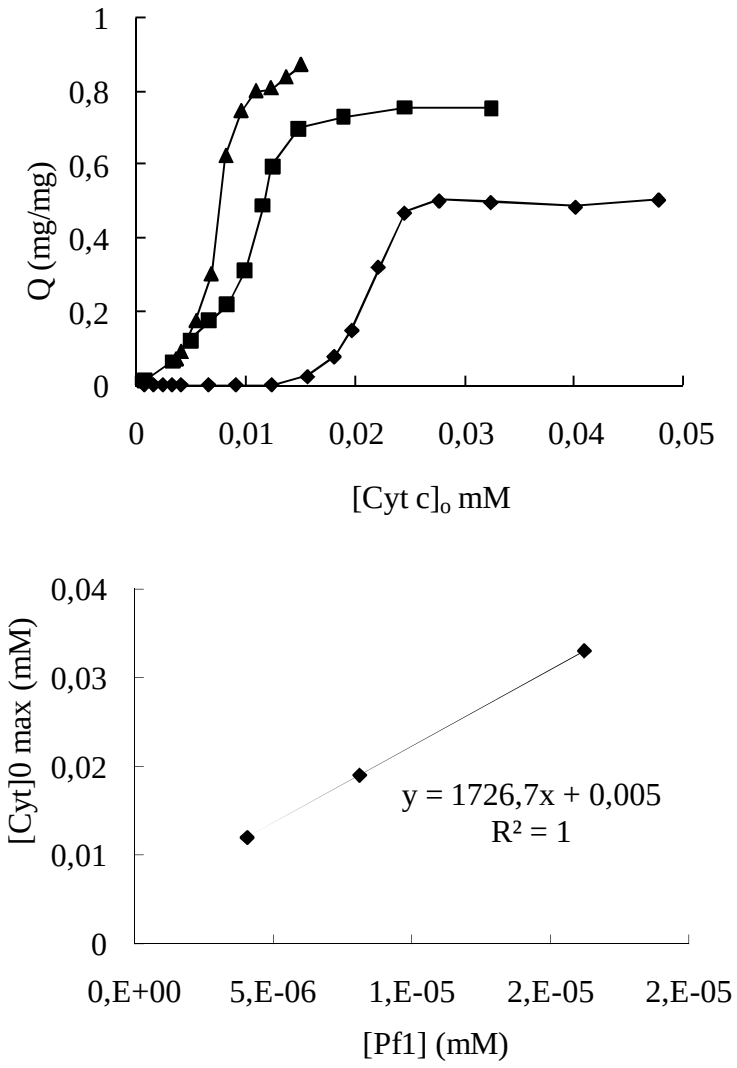

Figure 2.2 - a) Amount of complexed cytochrome c per mol of the Pf1 virus against the initial concentration of cytochrome c in solution. Phosphate buffer 2mM, pH 7, Pf1: (▲) 0.15mg/ml, (■) 0.25mg/ml and (♦) 0.6mg/ml. The concentration of cytochrome c corresponding to the highest value of capacity Q on each plot was visually determined, and it was plotted in **b)** as a function of Pf1 concentration. The result of a linear fit is shown.

The slope value of 1727 indicates that about 1700 cytochrome c molecules were restricted to near the Pf1 surface per one Pf1 particle. This result is on suitable agreement with the isoelectric aggregate, comparing to the charge balance.

2.2. Effect of salt addition on Pf1-Cytochrome c stability

Monovalent ions effect on the binding of polyvalent counterions to the charged macromolecular surface has been referred on counterion condensation theory. Such effect of monovalent salt can be probed through the light scattering measurements of bundle formation.

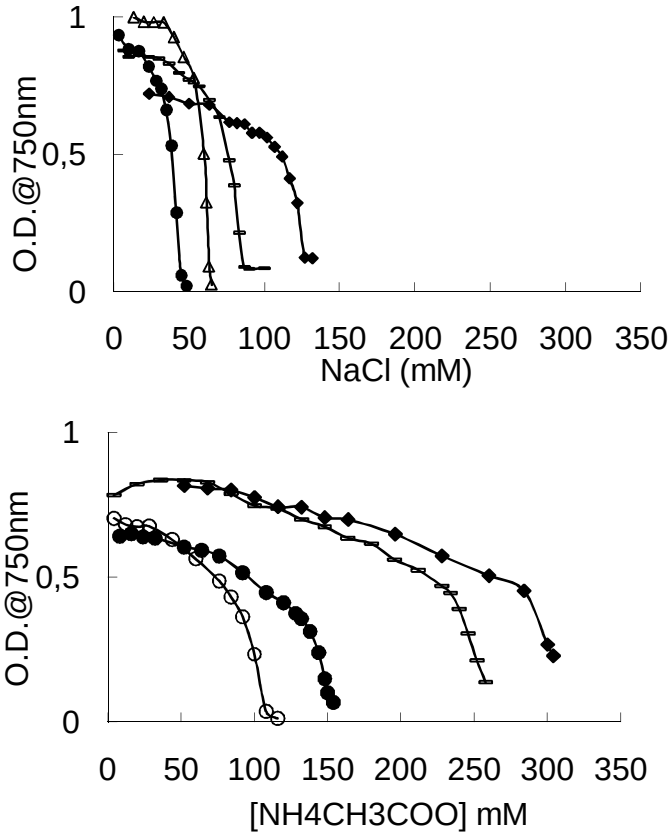

Figure 2.3 – NaCl and NH_4CH_3COO effect on Pf1/Cytochrome c complex stability. Concentrated salt solution was added in order to set the final ionic strength. Cyt c/Pf1 mass ratios showed in: (1) Fig. a): (•) 1/1, (Δ) 7/1, (□) 15/1, (♦) 30/1 and (2) Fig. b): (○) 2/1, (•) 9/1, (□) 44/1 (♦) 87/1.

A series of light-scattering measurements was performed to illustrate the stability of bundle formation as a function of ionic strength. First, concentrated cytochrome c was added into Pf1 solution and then salt was sequentially added into the solution. This enables to find the critical concentrations of salt required to disrupt the complex. The ionic strength-dependent behaviour is shown in Fig. 2.3, for both NaCl a) and Ammonium Acetate b).

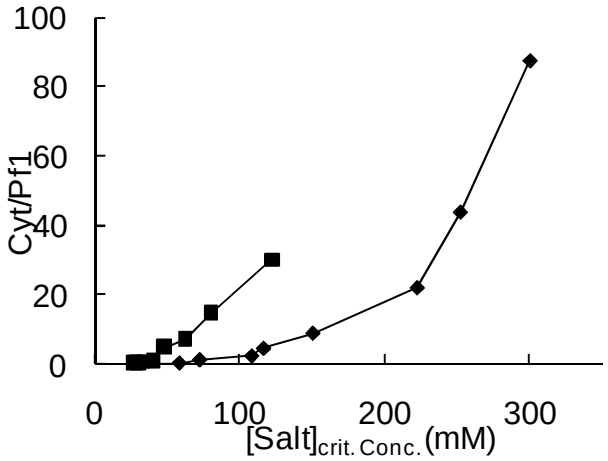

Figure 2.4 - Relationship between Cytochrome c/Pf1 ratio and two different salt dissociation were used: (•) Amonium acetate (■) Sodium chloride.

Experimental data show a sharp decrease in the light scattering signal for a specific NaCl or AmAc concentration (critical concentration) depending on Cytochrome c/Pf1 ratio. This critical concentration was determined by the first derivative of the curves in Figure 2.3 (inflection point). The critical salt concentration that defines the stability of the complex has a dependence with the Cytochrome c/Pf1 ratios, as shown in figure 2.4.

2.3. The size of Pf1/Cytochrome c aggregates

Dynamic light scattering spectroscopy was used to measure the size of the aggregates of Pf1/Cytochrome c. The hydrodynamic diameter values reported in this study are based on the size distribution by scatter intensity. The DLS intensity was measured versus particles diameter for different Pf1/Cytochorme c mass ratios, Figure 2.5. As cytochrome c concentration increases, an aggregate with a hydrodynamic diameter of around 1000 nm become dominant with a decrease of the component with smaller hydrodynamic radius (Pf1 particles).

The Pf1 virus alone polydispersity index were 0.463 ± 0.021 and show one smaller population which can correspond to the broken virus[71]. The polydispersity index grow up to 1.000 when Pf1/Cytochrome c mass ratio were 3/1; 2/1; 1/1, suggesting nano-structures variation with a high molecular weight increasing. At this ratios huge aggregations were detected behind 5000nm, even "visible" to the eye, suggesting larger assemblies of macromolecules in solution.

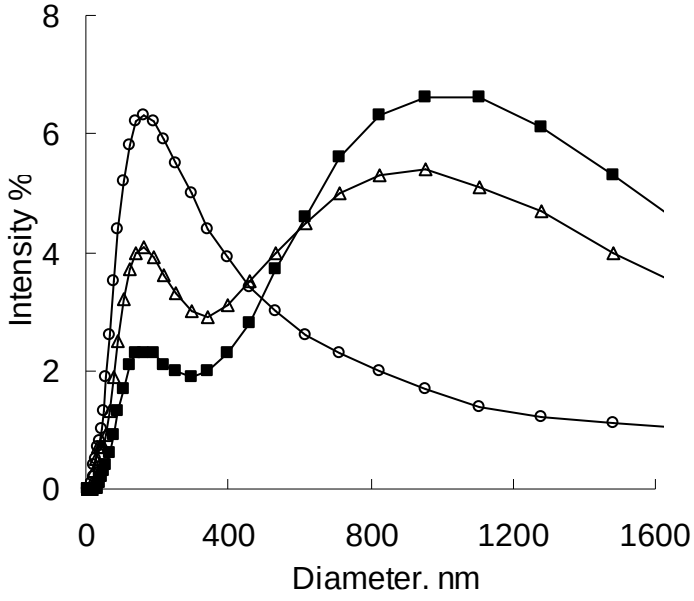

Figure 2.5: Dynamic Light Scattering Intensity (%) of Pf1 virus (0,1mg/ml) with Cytochrome c (10-100ug/ml) at pH 7.0 with different Pf1/Cyt c mass ratios: (○) 8/1; (Δ) 6/1; (■) 4/1.

2.4. Zeta potential measurements

Figure 2.6 shows apparent zeta potential increasing as Pf1 virus/Cytochrome c decreases ranging from 9/1 to 1/2. Pf1 and the mixtures were found negative charged between 1/1 and 9/1. As Pf1/Cytochrome c mass ratio decreases from 2/1 to 1/2, zeta potential grows up to approximately the same native zeta potential value of Cytochrome c alone (+6mV). In good aggrement with previously works[72]. The iso-electric point was exhibited around 0.6 (Pf1/Cyt c). Both protein and virus alone exhibit positive and negative zeta-potential respectively. This should not be surprising, as measurements were taken at pH 7.0, where that aggregation was observed at Pf1/Cytochrome c around 1/1 ratio .This seems to indicate that Pf1 have some of its negative surface charge characteristics changed by the cytochrome c influence.

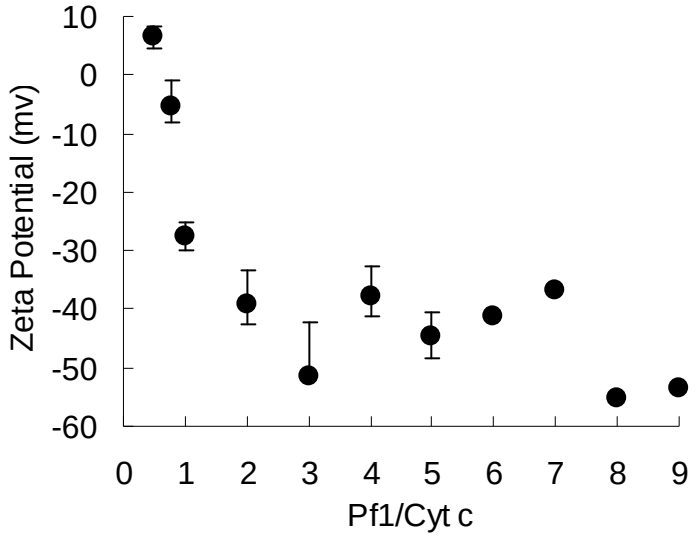

Figure. 2.6: Zeta Potential varying Pf1/ Cytochrome c virus mass ratios keeping the virus concentration at 0.1mg/ml, pH was adjusted using Phosphate buffer at 7.0.

2.5. pH influence on Cytochrome c /Pf1 complex

Zeta potential of Cytochrome c, Pf1 and the 1/1 mass ratio mixture were measured varying the solution pH from 2 to 12.5. Pf1 sample was strongly negatively charged between pH 11 to 6, with value potential of -46mV, until charge neutralization was accomplished at pH 3.7 and achieve +37mV potential at pH 2.8. At pH 2, cytochrome c exhibits a positive charge value around +6mV and led to a negative shift in the zeta-potential, with an inflection point near pH 8.5, with approximated -38mV potential value for higher pHs. The 1/1 mixture reveals a Pf1 net charge similar behaviour, increasing from -42mV potential at pH 10.2 to +47mV potential for pH 2.2 with an associated pI near pH 4.5. At pH 10, Zeta potential value was almost the same as Pf1 alone. Around pH 9.5 or higher no scattering were observed suggesting that no aggregation occurs.

To have an idea of charge behaviour of the particles involved in the aggregation, the pI was estimate assuming all residues to have pKa values that are equivalent to the isolated residues (Figure 2.7). For a folded protein this is not valid. However, this rough value can be useful for planning protein purfications.[73].

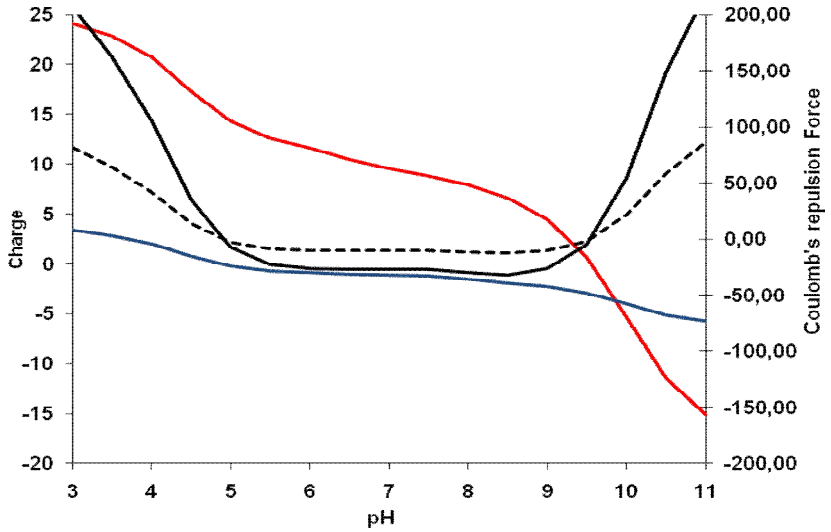

Figure 2.7: Estimated charge over pH range, were dashed point represent the product between Cyt c and Pf1; the black line the Cyt/Pf1 ratio; Red line represents the overall charge of the Cytochrome c and at blue the Pf1 virus.

Similar UV visible experiment were realized that supporting, were aggregations occur between pH 5.5 and 8.0 as expected, and at higher pH no complexes as been seen.

2.6. Atomic Force Microscopy

Samples of Pf1 virus and Cytochrome where prepared with and without Mg^{2+} pre-treatment of the in freshly cleaved mica. Samples were observed by atomic force microscopy in tapping mode. A series of experiments was performed using the liquid cell at different ratios of Pf1 bacteriophage and cytochrome c (figure 2.9). This result was dependent of the mass ratio of Pf1 and Cytochrome c and the concentration of ammonium acetate.

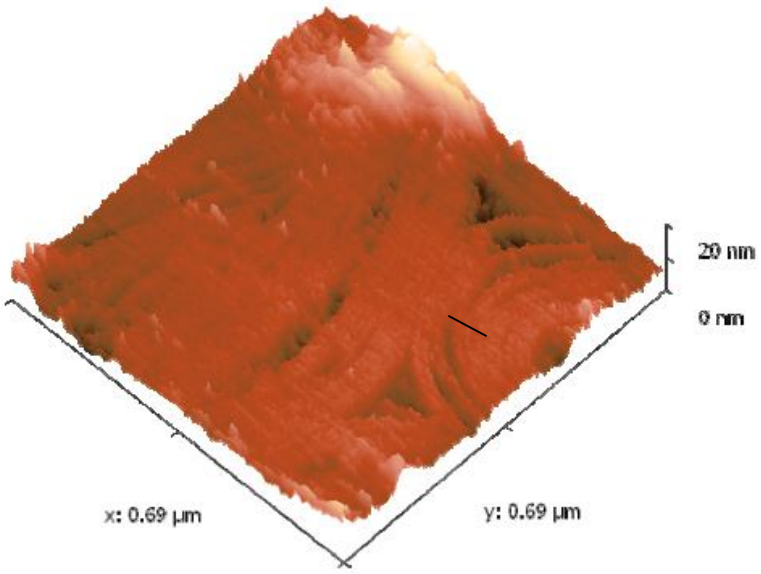

Figure 2.8 Atomic force microscopy images of Pf1 and Cytochrome c using the liquid cell with mass ratio 1:2 and 6mM ammonium acetate pH 6.8.

Results shows some regularity geometric forms and the distance value obtained between the two higher pick surfaces were 13.5 nm since cytochrome is about 3.3 nm diameter with is about half of the virus diameter (6.7 nm). So if we have two cytochrome c by sides and two virus (Figure 2.10), it is possible to explain the experimental obtained distance.

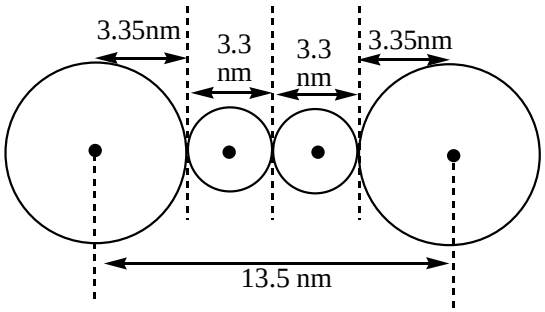

Figure 2.9: Surface representation of the samples obtained from figure 2.9, with the possible two cytochrome c molecules between two Pf1 rod virus environments.

2.7. NMR titration of Pf1 / Cytochrome c sample with NaCl.

A NMR sample prepared with 1:1 mass ratio of Cyt c: Pf1 virus at low ionic strength displayed aggregated complex suspension, expected for this experimental conditions. The complex stochiometry implies an 1/3 mass of cytochrome is not bounded to the aggregate.

The stochiometry of the complex was determined to be 2:3 mass ratio by UV/visible /centrifugation experiments. This correspond to an isoelectric electrostatic complex with an approximate empirical formula of Cyt c_{1700n} $Pf1_n$

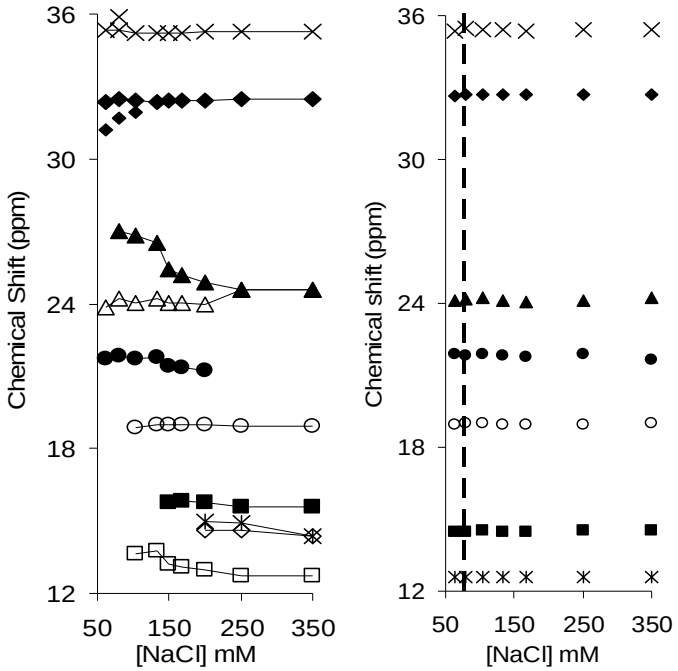

Figure 2.10 **(A)** - Left - Low field Cytocthome c NMR signals of the of Cytochrome c/Pf1 virus on mass ratio 1:1 (20mg/ml) of the titration with NaCl salt [3.3 to 350]mM**. (B)** - Right - Same conditions and procedure without Pf1 virus. Heam - HM8(×), HM3:(♦), HA71(○); His18 – HB1(■), H4(▲), (Δ) and maybe (•); H2(-); Met 80 HB1(□) and/or (*),(◊)[74].

In the low salt content conditions we see a low intensity NMR spectra, with resonances significantly deviated to the ones observed in the cytochrome c sample without Pf1 virus. The stepwise increases of added salt (NaCl) induce dramatic variations in terms of both chemical shifts, linewidths and spectra intensity. (Figure 2.10 and 2.11). A control salt titration (without Pf1 - figure 2.10 B) show that the variation of NaCl concentration don't affect the spectra of Cyt c spectra.

The increase in the spectra intensity is due to the dissociation of the aggregates that release of cytochrome from the complex (see figure 2.11).

It is important to notice that the cytochrome c NMR spectra at low ionic strength indicate that there is a dynamic binding/unbinding equilibrium between free and associated complex in the NMR time scale.

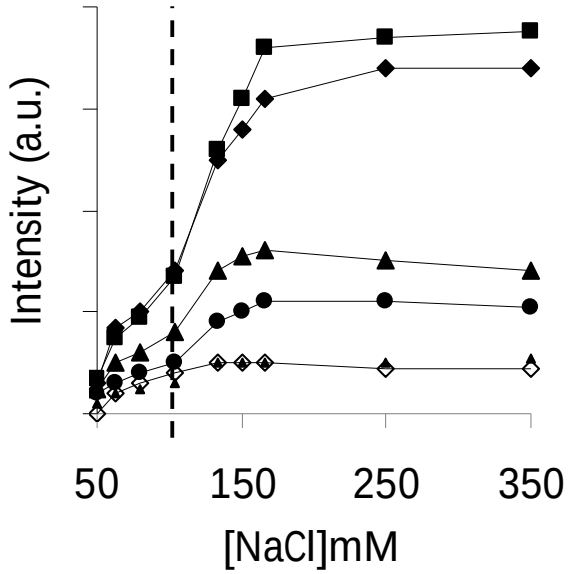

Figure 2.11 - Comparison between the ^{1}H-NMR peaks intensity of Cyt c with Pf1 at ratio 1:1 increasing NaCl concentration. Haem - HM8(■), HM3(♦), HA71(•), HA72(▲); His18 – HB1 (◊), H4 (*), (Δ) and/or (○); Met80 – HB1(□).

The results of the NMR salt titration at high ionic strength are comparable with the observed spectra in the absence of Pf1 virus. Although some chemical shift differences remain even at 500mM NaCl indicating that some perturbations persist even at high ionic strength. The broadening of the resonances verified al low ionic strength can be attributed to field inhomogeneity and cytochrome c rotation hindrance. Microscopic viscosity that could cause broadening of resonances should be cause this variation having in mind that the total amount of Pf1 is increase during the titration upon complex dissociation.

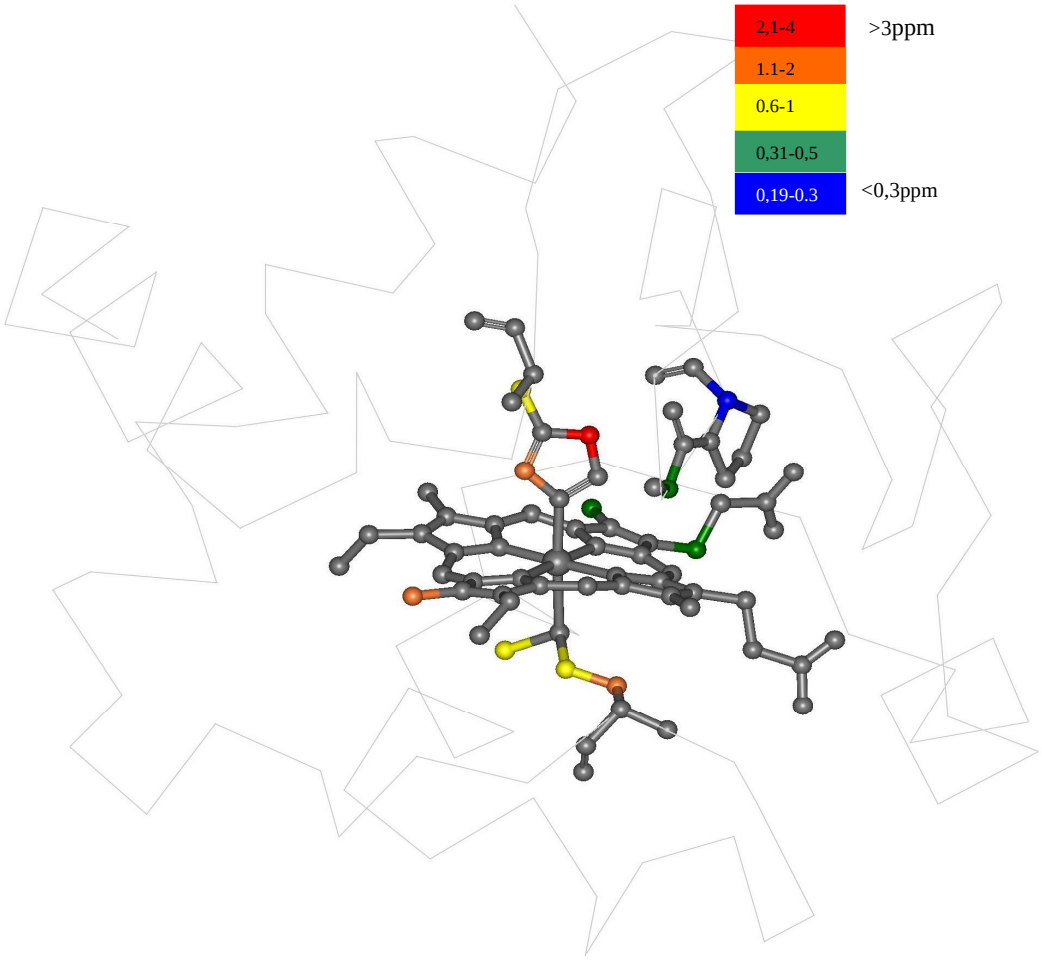

Fig. 2.12 Colored identified peak show the chemical shifts deviations between 0,19 to 3,7 ppm on a logarithmic scale. The heme, along with amino acids with assigned peaks are shown in gray.

2.8. DOSY – Titration of Cytochrome c with Pf1 virus at 150 mM

In high salt constant concentration conditions, the stepwise increases of added Pf1 induce a dramatic apparent self diffusion decrease of the cytochrome c with significantly deviated to the one observed in the cytochrome sample without Pf1 virus. With the approach of the Cyt c/Pf1 stoichiometry inversely the apparent hydrodynamic radius calculated increase (see Eq. 1.1). In fact the real radius of cytochrome c do not increase. But the proteins interaction with the Pf1 virus change their free mobility following a tendency to look like the PF1 virus mobility, that is invisible to NMR spectroscopy - due to the high tumbling time. It is important to keep in mind that at this ionic force no aggregation/sedimentation can occur between the proteins and particles.

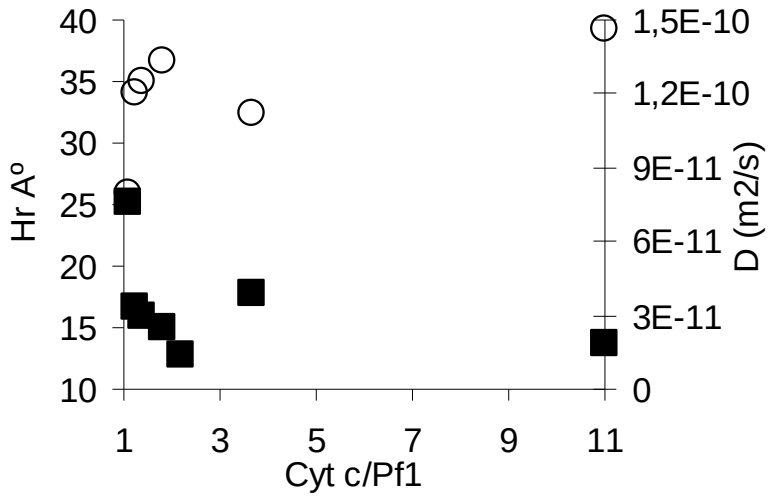

Figure 2.13 – Self diffusion of Cytochrome c in presence of Pf1 at various ratios. At left YY axis (○) Diffusion coefficient and at right the calculated equivalent (■) Hydrodynamic radius.

2.9. Mass ratio calculation of Cytochrome c and Pf1 virus

2.9.1. Geometric calculations of the ideal mass ratio Cyt c versus Pf1

This section was entirely and brilliantly developed by Dr. Jorge Caldeira that i want to thank. This tool has brought a great help to understand how a geometric aggregation between Pf1 virus and Cytochrome c. One way to estimate the maximum protein that can spatially aggregate to the virus is considering the protein as geometrically forms (rod and sphere, respectively). Also, only one layer is considered occupied around the virus:

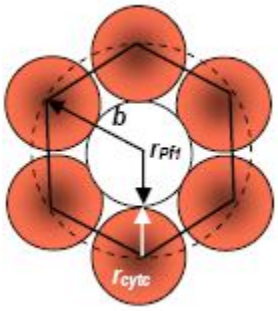

Figure 2.14 - top (or bottom) view representation of the maximum protein packing about the virus surround knowing the perimeter for the circle:

By the figure 2.14 is possible calculate the perimeter results by:

$$P_{circle} = 2\pi b, \text{ (eq. 2.1)}$$

where b is the sum of the radius of the virus and cytochrome and it is the distance between the center and one of the vertices of the polygon to:

$$b = r_{cyt} + r_{Pf1} \text{ (eq. 2.2)}$$

Hence, perimeter for regular polygons is given by:

$$P = 2nb\sin\left(\frac{\pi}{n}\right) \quad \text{(eq. 2.3)}$$

Where n is the number of sides (number of cytochromes around the virus). The calculation of proteins packed vertically along the virus can be estimated considering the virus as a rod and its section height **h** that can have a ring of cytochromes defined as:

$\mathbf{h}_{sq}$= 2* $r_{cyt\ c}$ for square packing and $\mathbf{h}_{hex}$= 2√ ¾* $r_{cyt\ c}$ for hexagonal packing (figure below).

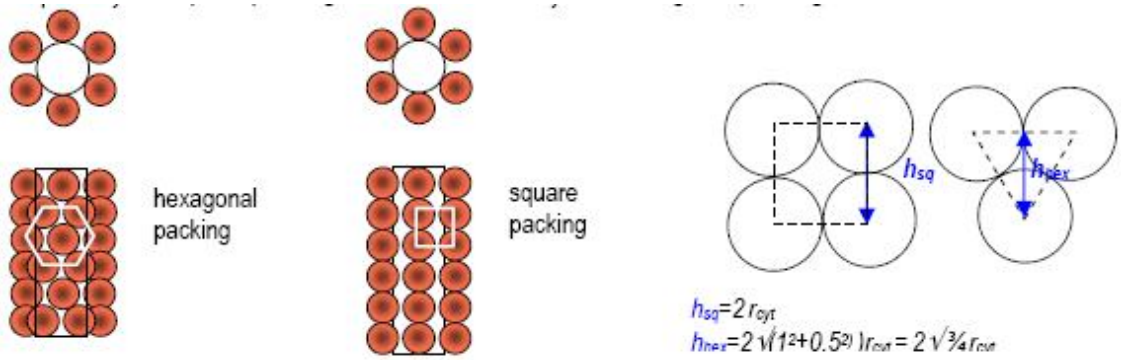

Figure 2.15 - Left: Hexagonal and square packing were the rectangle rod represented as the Pf1 virus. Rigth: square and triangular geometric representation resulting of the hexagonal and square packing of Cytochrome c around the Pf1 virus.

As first observation the hexagonal packing is more densely packed than square packing

hsq = 2 Rcyt hhex = 2 x 0,8660 Rcyt (eq. 2.4)

Tacking this result it is possible to calculate the mass ratio of maximal load of cytochromes in the virus surface assuming:

$$\frac{Mass\ \ Cyt\ \ c}{Mass\ \ Pf1} = \frac{Volume\ \ Cyt\ \ c}{Volume\ \ Pf1\ \ c} = \frac{R_{cyt\ c}}{R_{Pf1}} \quad \text{(eq. 2.5)}$$

This can be calculated for a section of virus of height h

$$Volume\ \ Cyt\ \ c = n \times \frac{4}{3} \times \pi \times R_{Cyt\ c}{}^{3} \quad \text{(eq. 2.6)}$$

$$Volume\ \ Pf1 = \pi \times R_{Pf1}{}^{2} \times h_{hex} = \pi \times R_{Pf1}{}^{2} \times (2 \times 0.866 \times R_{Cyt\ c}) \quad \text{(eq. 2.7)}$$

$$R = \frac{n \times \frac{4}{3} \times \pi \times R_{Cyt\ c}{}^{3}}{\pi \times R_{Pf1}{}^{2} \times \left(2 \times 0{,}866 \times R_{Cyt\ c}\right)} \quad \text{(eq. 2.8)}$$

Were n is the number of cytochromes around the virus

Expressing n in terms of rcyt and rPf1 $P = 2nb\sin\left(\frac{\pi}{n}\right)$ (Perimeter of polygon)

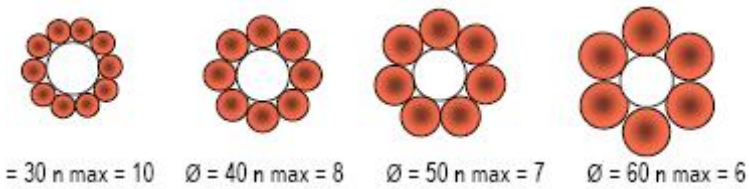

Figure 2.16 – Representation of the cytochrome quantity around Pf1 perimeter.

But, the perimeter is also equal to n* 2 rcyt one diameter (2 rcyt) corresponding to one side of the polygon

$$Ppolygon = 2nb \sin(\pi/n) = n*2*rcyt \quad \text{(eq. 2.9)}$$

b is the sum of the radius of the virus and cytochrome b = rcyt + rPf1 and n can also be expressed in terms of rcyt and rPf1, solving the equation above:

$$Ppolygon = 2n(rcyt + rPf1) \sin(\pi/n) = 2nrcyt$$

$$Ppolygon = (rcyt + rPf1) \sin(\pi/n) = rcyt$$

$$Ppolygon = \sin(\pi/n) = rcyt /(rcyt + rPf1)$$

$$\arcsin(\sin(\pi/n)) = \arcsin(rcyt /(rcyt + rPf1))$$

$$(\pi/n) = \arcsin(rcyt /(rcyt + rPf1))$$

$$1/n = \arcsin(rcyt /(rcyt + rPf1)) / \pi$$

$$n = \pi / \arcsin(rcyt /(rcyt + rPf1))$$

Then:

$$R = \frac{\pi}{\dfrac{arc\ \sin\left(\dfrac{R_{Cyt\ c}}{R_{Cyt\ c} + R_{Pf1}} \times \dfrac{4}{3} \times \pi \times {R_{Cyt\ c}}^3\right)}{\pi \times {R_{Pf1}}^2 \times 2 \times \sqrt[3]{\sqrt{R_{Cyt\ c}}}}} \quad \text{(eq. 2.10)}$$

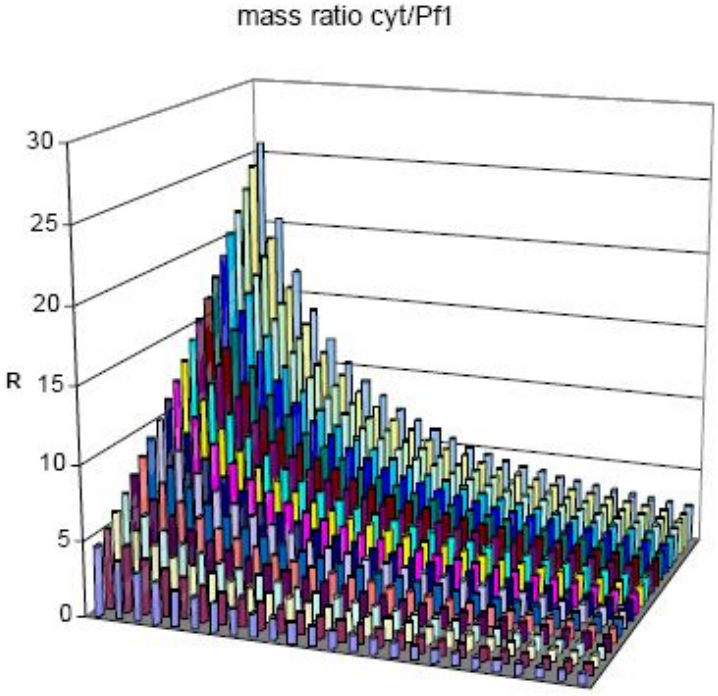

Figure 2.17 - Ideal cytochrome c /Pf1 mass ratio based on virus diameter and protein radius according to the derived equation.

From this theoretical equation it is possible to compare the stoichiometry calculated by UV-visible; DLS or AFM experiments results.

3. DISCUSSION

3.1. Stoichiometry of Pf1 virus cytochrome c complex

A set of UV-Visible experiment was carried out, centrifuging various Pf1/Cyt c mass ratio proportions and then adding NaCl at increasing concentrations, between 0 and 200 mM with total solubilisation. This is in agreement with the fact that Coulombic interactions drive the association between the virus (polyelectrolyte) and a protein of opposite charge. At the stoichiometry, the amount of cytochrome c condensed also depends on the quantity of added salt and is larger for small concentrations of the last one (figure not show). The special conditions that lead the precipitation process at a specific stoichiometry depending on the gain in the entropy due to the liberation of low molecular couterions (such $PO4^{2-}$; Na^{+}; Cl^{-}) from the environments chains of Pf1 and Cyt c around. When other ratios, non stoichiometric, were prepared even with a small complex precipitated, the cytochrome c cannot condense onto the polyelectrolyte until the charged density between neighboring chain charges along with the virus is reduced below a certain critical value.

3.2. Ionic strength

The presence of a small amount of salt enables rearrangement to thermodynamic equilibrium, leading to a uniform distribution of the components among all long chains of the virus. We have studied the reversible transition from a solid aggregate to a free flowing liquid depending on salt concentration. At higher salt concentration the precipitate dissolves and both components exist as free polyelectrolyte and protein in solution. Similar effects can be induced by changes of the pH value. The presence of NaCl led to a dramatic decrease of the level of aggregation for Pf1/Cyt c. The enabled rearrangement processes make the salt a decisive part in the formation of highly aggregated. The level of aggregation can be controlled by the amount of salt during complex formation that can lead us to tunable degrees of alignment by with salts concentrations.

The ionic strength dependens on varying the Cyt c/Pf1 ratios (Figure 2.4), showing a linear behaviour to some extent. At higher Cyt c/Pf1 mass ratio small increase of salt is needed to break the complex. The complex formed is stable on solution with no precipitates due to electrostatic force that prevents the precipitation. Monovalent salt competitively interacts with the charged filaments and acts to reduce the attractive interaction mediated by the Cytochrome c. The linear behaviour dependence of salt and cytochrome c added can be explained by the counterion stabilization of the charged cytochrome c in excess (the stoichiometry of the complex don´t change). At higher charge density solution less salt need to disrupt the complex because of tendency of the Cyt c to stay on the complex (Cyt c on bulk is

on excess). The differences between the AcAm and NaCl are essentially the size. NaCl is much smaller and can break easily the complex. Larger diameter ions are less able to mediating attractive forces, considering hydrated ion size.

There is a entropy tendency to maintain cytochrome c in the middle of the solution (bulk) and not aggregated. When a huge amount of protein (positive charges) is in the bulk the cytochromes tendency to escape from the complex is lesser.

An interesting model developed by Alexander Lyubartsev et al predicts this phenomenon with suitable agreement to the proportions of the experimentally data obtained. The model is made by three triangular parallel charged rods (representing the Pf1 virus) at a fixed distance, making a structured box with various proportions of countercharge sphere (representing the cytochrome c) and a variation of the ionic force. (infinite length and finite charge density- see pag 20). The effective force between the ordered rods is directly related to the osmotic pressure in the rod system. Since the osmotic pressure of the bundle rises more rapidly as a function of salt concentration than the pressure of an aqueous solution at the same concentration, allowing the osmotic pressure to balance the bundle pressure as salt concentration increases. The exclusion of salt from the bundle is in turn driven by a complex interplay of entropic effects and electrostatic interactions.

However the model does not take into account the molecular details of real polyelectrolyte and protein chains, like e.g. local solvation effects, atomic partial charge distributions and other characteristics related to the organization of complex.

3.3. DLS discussion (force; size;polydisperse)

Experiments were carried at various Pf1/Cytochrome c mass ratios. Population of the Pf1 virus decreased, in favour of the increasing population with average size between 712 and 1200 nm, which suggests the spontaneous formation of Pf1/Cytochrome c aggregates. Since the interaction between the protein and the virus is of electrostatic nature, the effect of ionic strength on the titration curves of Pf1/Cytochrome c (1:1 mass ratio) by NaCl was, then, evaluated. A decrease in the scattering intensity value is induced by the increase of ionic strength leaving to approximate the hydrodynamic radius of the unbounded Pf1 virus, suggesting a reversible system. (similar to UV-visible experiments).

Even though samples were centrifuged to isolate the contribution of the large aggregates from the size distribution histograms, their extensive contribution for the scattering signal prevented the utilization of data obtained. It is possible to observe perturbations on the scattering intensity even at 6/1 (Pf1/Cytochrome c mass ratio) where the complex appears with a hydrodynamic diameter varying between 712 and 1200 nm and intensely around 1000nm (figure 2.5). Near the stoichiometric ratio, at

3/1 and higher, Pf1/Cytochrome c mass ratio (polydispersity index > 1) the complex appears on quantity enough to mask the free Pf1 virus, or no more unbounded Pf1 virus are available on solution. (remember that the scattering of one particle is proportional at the hydrodynamic radius^6). On other hand, the source of polydispersity index is also reinforced by the presence of at least two Pf1 virus populations (1um and 2um) on solution. When the stoichiometry is reached a huge molecular weight increases. The generation of new complexes is the dominating process with increasing mixing ratio, not a growth of the Pf1 complex. The sharp rise in light-scattering intensity at the transition of bundle formation suggests that aggregation tends to proceed to form large bundles were all Cyt c on solution as involved. However, because the formation of small bundles precedes that of larger ones, the formation of small bundles as the necessary initial step may pose a kinetic barrier for the formation of large bundles aggregations.

Extension ratio range analyzes leads to many problems; decreasing the Pf1 concentration a not able system is created for the equipment detector, on other way absorption at 633nm laser from Cytochrome c is increase with the concentration.

3.4. Zeta potential discussion

On this system, the positive particle is the protein and the aggregation behaviours depend on the nature of the ionic groups of virus chain and salt. The high charge density, along with the virus rod produces a high electrostatic potential around it, and counterions are located in the immediate vicinity of the virus rod. The amount of protein (considered as a charged polymer) adsorbed at the Pf1 surface also changes the charges surface which are related to a magnitude surface potential. It is expected that as this amount increases, the surface charge will vary until it attains a stable value, indicating that no more protein is being adsorbed. In fact, Zeta-potential is related to the surface charge of proportion of absorbed protein molecule that is exposed to the solvent.

ζ-potential data demonstrated the aggregation by an increase of the Pf1 negative surface potential observed when incubated with increasing amounts of protein. The ζ-potential acquired in solution in aggregated conditions (Figure 2.6) follows a neutral charge as the protein concentration increases, indicative of the formation of a protein layer(s) at the Pf1 surface. The ζ-potential increase from 1:3 to 2:1 where the system have an enthalpy gain, by other words the stoichiometry is reached. Evidently at 1:1 ratio, precipitation was observed on the corner corvette suggesting large bundles, so the stoichiometry was reached. The I. p. arrive at 0.6. Between 1:3 to 1:7 the ζ-potential show variations suggests small bundles formation with polydispersity aggregated (between -36 to -53), in good agreement with DLS results. However the diffusion for a rod virus particle can also have a preferential path. For example, lateral diffusion is less probably than diffusion obtained by the end to end

travelling virus due to the higher friction factor, meaning that the ζ-potential values obtained by calculations methods may contain associated errors.

3.5. pH discussion

Important parameters that will be investigated in future research include the Cytochrome c surface charge density (which can be controlled by variation of the pH) as well as the Pf1 virus charge. That charge density can be characterized by changes on zeta potential. The Pf1/Cytochrome c 1/1 mass ratio mixture at pH 3 buffer has highly positive zeta potential value which indicates that no aggregation occurred. If more alkali is added to the aggregated species, the positive charge of Pf1 virus neutralizes to a negative charge ranging from pH 4 to 12. This result indicates that aggregation occurred about this range of pH. At pH about 10 no aggregation was observed, with potential zeta value approximately the same as free Pf1 virus. As a result, the aggregation at pH 5.5 to 8.5 results in an unstable complex system. At pH higher than 9 a stable system occur with no aggregation.

To well understand what happened when pH is into play AFM was very helpfully. Figure 2.8 and 2.9 show the pH influence. The liquid crystalline packing of the virus in the liquid mode was much more aligned that the dried sample at the identical pH, suggesting that electrostatic virus–virus repulsion is considerable smaller due to water dielectric properties. On dry mode all components such: salt, phosphates and residual water have completely different properties.

3.6. Chemical shift discussion

The chemical shifts of the methyl heme and axial methionine resonances are very sensitive to small structural and electronic perturbations in the vicinity of the heme groups. The observed chemical shifts are dependent on both contact and pseudocontact terms, which are dependent on the spin densities of the paramagnetic heam.[51]. A tridimensional representation of the observed variation in chemical shift around the heam group is presented on figure 2.12.

The poorly resolved spectrum of the cyt c less than 50mM of salt tells that strong electrostatic interactions with Pf1 anion and Cyt c strongly hinder rotation. Broadened lines appear on all resonances until about 91mM of NaCl, and after that just some shifted peaks (4 or 5) continuo very broad. The splitting of the resonances of heme methyls 1, 5 and 3, and the broadening of 8CH3 indicates the presence of a further species at low ionic strength. In addition to broadened lines, the signals H4; HB1 of His18; 29alfa of Gly, and HM8, HM3 of Heme are splitted. This splitting of resonances and the broadening indicate the presence of a further specie on the sample. Even at higher charge density solution (>250mM of salt) the electrostatic radius Pf1 virus influences have a great contribution for intensity and chemical shift of Cytochrome c protein.

3.7. DOSY discussion

DOSY NMR spectroscopy is particularly useful to describe the dynamic behaviour of cytochrome c in our complex aqueous solution. The titration with a sample of pure cytochorme and increased the amount of Pf1 until a 1:1 mass ratio (pf1 and cytochrome c). The pH and ionic strength are a crucial parameters to define the binding in mixture of Pf1 and cytochrome were set to pH 7.0 and 150mM of NaCl. In these conditions no aggregate is observed and salt concentration is just above the critical concentration of Pf1 binding (50-100 mM depending on cytochorme and virus concentration). Therefore a free liquid solution was obtained through all the Pf1 titration and since Pf1 and cytochrome have 3000 fold difference in terms of molecular mass, the associated complex observable in liquid state NMR, being the experiments based only in the cytochrome free molecule. Besides this fact the strong attraction between the nematic and magnetically aligned virus and the cytochrome can still be observed in the DOSY experiments of in the chemical shifts perturbation even at higher salt concentration higher than the critical concentration of complex formation.

Therefore we conclude that a free remaining cytochrome c at low ionic strength is in transient exchange mode with the aggregate complex in suspension.

3.8. Discussion; AFM and geometric mass ratio calculations

From the maximum cytochrome c geometric able to be around the Pf1 virus we can take the literature dimensions for example: $R_{cyt\ c}$ and P_{Pf1} of 1.7 and 3.4 Ang. respectively, the Cyt c/Pf1 mass ratio obtained for this radius was around 1.6 equivalent to the maximum of 10 cyt c /Pf1 (Figure 2.17). To have the mass ratio on properly consistence with the stoichiometry, we need to select: R_{Pf1} = 4.3 Ang. or higher and $R_{cyt\ c}$ = 1.1 Ang. or less, which is physically impossible. Suggest that behind the cytochrome c aggregated directly around the virus influence, it can affect the cytochrome c surrounding and when entropy is balanced the aggregation occur. In DLS experiments (Figure 2.5), a simplistic observation that the complex size is five times higher than free PF1 particles. Near the stoichiometry (between 3/1 to 1/1) the size complex increase and also the molecular weight of populations.

Furthermore on NMR experiments, high concentrations of Pf1 and Cyt c on system, not compatible for techniques such: DLS or zeta potential (diluted solutions), turn the complex more compact introducing the nematic factor (mechanic force). The kinetics and stability of the bundle formation requires consideration of many physical effects: structural geometry, bond rotation potentials, and steric interactions between near-neighboring groups and excluded-volume interactions become more prominent and the occurrence of polyelectrolyte-macroion complexation is governed by the interplay

between these short-range potentials and the electrostatic interactions. nematic phase combined with special orientation induced by magnetic field, leading us to a fascinating subject: The alignment of molecules, since in induce the comprehension of structure spectroscopy relations, enables the study of complex molecular interactions and help in the fabrication of ordered materials with numerous practical applications. Shape and charge irregularity common in protein molecules make them very hard to align with a high order ($S \geq 0.1$) parameter. Furthermore this knowledge offers the promise of rational construction of interesting materials and useful novel spectroscopic applications.

4. CONCLUSIONS and FUTURE WORKS

The aim of this work was to explore the experimentally accessible parameter space (pH, salt, etc.) in order to create materials that impose a maximal alignment order a metaloproteins.

Pf1 vírus and cytochrome c are oppositively charged ranging from 4,5 to 9,0 pH to promote the formation of strong electrostatic complexes with a concrete stoichiometry. The complex precipitates from aqueous solution at low ionic strength forming an isoelectric complex.

The interaction of polyelectrolyte solutions containing Pf1 polyanions and cationic Cytochrome c protein has been studied. The formation of complex from oppositely charged chains has been observed for a critical Pf1/protein ratio. Complex stability is dependent of salt concentration, and disaggregation occurred when salt concentration increases.

With this work, conditions for complex formation of Pf1 and Cytochrome c protein were found and will be useful to explore orientation of proteins in future work. Genetic engineering can be also applied to Pf1 virus to change the surface charges and construct other building blocks for other proteins. Fibrils can be also easily be fabricated and study of the protein orientation induced by the Pf1 virus.

5. MATERIALS and METHODS

5.1. MATERIALS

Filamentous Pf1 bacteriophages (50±4 mg/ml) were purchased from ASLA Biotech RĪGA Letónia and were used without further purification. Horse heart cytochrome c (>99%) and all other chemicals were obtained from Sigma Aldrich with the highest purity available.

5.2. METHODS

5.2.1. PROTEIN PURIFICATION

Cyt c, was chromatographic purified using a Merck L-7100 HPLC equipped with an L-7400 UV detector and D-7000 computer interface, with a cationic exchange column resource-S (GE Healthcare) with a linear NaCl salt gradient at pH 7.0, and collected and concentrated and permuted to the desired buffer conditions using 10 KDa cut-off centricons (Vivascience).

5.2.2. EFFECT OF SALT ADDITION ON Pf1-CYTOCHROME C COMPLEX STABILITY.

The effect of salt concentration (NaCl and ammonium acetate) was performed with varying salt concentration from 0 to 350 mM. Experiments were done for different cytochrome c/Pf1 mass ratios. The solution was gently stirred for 2 minutes to attain equilibrium at room temperature (25ºC). Light-scattering measurements were then performed (at 750nm) in a Shimadzu, 2101PC UV-Visible scanning spectrophotometer.

5.2.3. CYTOCHROME C TITRATION OF Pf1 SOLUTIONS.

Pf1titration were made using 0.15mg/ml, 0.25 mg/ml and 0.6 mg/ml of Pf1. Phosphate buffer, without salt, solution was added to a final concentration of 2mM to 1ml cell volume in order to have a pH of 7.0. Cytochrome c was stepwise added in order to have increasing cytochrome c concentration inside the cuvette. After each cytochrome c addition the solution was magnetically stirred for 5 minutes. Then, the solution was centrifuged at 14000rpm for 5 minutes to precipitate the complex, and the supernatant was carefully removed. The cytochrome c concentration in the supernatant was determined by UV-Visible spectroscopy at 410nm. The supernatant was then added to the pellet,

mixed and more cytochrome c was added. This procedure was repeated until the cytochrome c concentration reached ~1 mg/ml.

The amount of cytochrome c bonded on Pf1 was determined with the equation:

$$Q= [(C_i-C_f)V]/m \text{ (eq. 5.1)}$$

where Q is the bonded capacity (mg/mg); V= 1ml the volume, C_i and C_f the cytochrome c concentration in the initial and final solution (mg/ml); and m the mass of Pf1 (mg). The capacities were plotted against the initial cytochrome c concentrations (Ci).

5.2.4. COMPLEX SIZE MEASUREMENT

Cytochrome c was treated with K_3 [$Fe(CN)_6$] and 0,05 % of NaN_3 , stored at 4 ºC. Samples were prepared to have the final phosphate buffer concentration of 0.2mM at pH 7.0 and the final cytochrome c concentration were varied from 0,01 to 0,1mg/ml with Pf1 virus kept at 0.1mg/ml. The complex mixtures were prepared diluting the protein into 1ml of buffer and filtered through a 0.45µm nylon filter membrane (GD/X 25, Whatman). The solutions were transferred to a disposable cuvette (DTS0012- Disposable sizing cuvette (1ml), Sarstedt), where Pf1 virus was directly added up. Samples were centrifuged for 10 minutes at 1000rpm and incubated for 10 minutes at 25ºC. Measurements were collected at a scattering angle of 173º using a Zetasizer Nano ZS instrument (Malvern) with an incident laser excitation at 633nm. Each sample was measured at least 12 times and each measurement consisted of 70 acquisitions.

The correlation time function of the scattering intensity for each sample was analysed with the DTS software supplied with the instrument by means of the inverse Laplace transform program CONTIN, and the hydrodynamic diameter was calculated by the Stokes-Einstein equation.

5.2.5. ZETA POTENCIAL

The same instrument Zetasizer nano were used to calculates the zeta potential. pH values were measured and adjusted using NaOH and HCl before sample measurement through the disposable zeta cell with a potential applied of 40V. Cytochrome c stock was diluted and filtered trough a 0.45µm pore size filter to a final concentration range from 0,009 mg/ml to 0,19mg/ml. Pf1 was added unto a final concentration of 0,1mg/ml to a final volume of 1ml. Zeta potential was calculated using DTS that is related with the electrophoretic mobility data sample obtained

5.2.6. NMR TITRATION OF Pf1 VIRUS /CYTOCHROME C SAMPLE WITH NaCl.

Cyt was kept oxidized with 10mM $[Fe(CN)_6.K_3]$ and permuted with 10mM Na_2HPO_4, pD=7.0 deuterated buffer with a final concentration of 20 mg/ml. The Pf1 virus was added to a final concentration of 20 mg/ml. Salt titration of Pf1/Cyt c (1:1) mixture was performed stepwise adding NaCl (in D_2O) to a final concentrations ranging from 8 to 500 mM. A control salt titration of Cyt c without Pf1 virus was done in the same conditions. The samples were kept in 5 mm NMR tubes at 4ºC prior to measurements.

5.2.7. DOSY NMR TITRATION OF CYTOCHROME C AT 150mM OF NaCl SAMPLE WITH Pf1 VIRUS

Samples for DOSY NMR were prepared as above with Cyt c, oxidized with $[Fe(CN)_6.K_3]$ 10mM in the presence of 150mM of NaCl, Na2HPO4 10mM, pD = 7,0 in D2O to a final protein concentration of 16,6 mg/ml. Pf1 virus was added to a final tube concentration varying from 1,5 mg/ml to 17 mg/ml. PEG 6K were used as Internal reference

DOSY NMR experiments were recorded at 25ºC on a Bruker AVANCE, AQS400 spectrometer operating at 400 MHz equipped with a Bruker multinuclear z-gradient inverse probe head capable of producing gradients in the z direction with a strength of 50.3G cm-1. The pulse sequence used for the diffusion measurements was the ledbpgppr2s sequence and the HOD residual signal was suppressed by means of a soft presaturation. The gradient pulse strength (g) was varied in 32 linear steps from 95% until to 2% of the maximum gradient strength. In these experiments, gradients were calibrated against the HOD diffusion constant at 25 ºC (D2O, 99.9%, $D = 1.9 \times 10^{-9}$ m^2 s^{-1})[75]. In this sequence based on a stimulated echo, the gradient pulse duration (δ) and the diffusion delay (Δ) were kept constant, at 1.5ms and 0.7s. Spectra with 32scans were measured at 25 ºC with a 90º pulse duration of 10.07 µs and a relaxation delay of 1s. The longitudinal eddy current delay was held constant to 5 ms.

5.2.8. ATOMIC FORCE MICROSCOPY DATA (Aligned metalloproteins with magnetically oriented virus)

Materials were prepared in a special alignment cell. In this cell the sample compartment is enclosed by a dialysis membrane that traps both the protein and the virus, allowing variation concentration of other small molecular weight components by connection to an outside chamber. Several inlet/outlet circuits were designed and operated by a peristaltic pump/vacuum pump in order to program a sample preparation protocol. Experimental variable such us: salt concentration, pH, temperature, pressure (vacuum) can be altered in both the sample and the dialysis chambers while being inside the 50 mm bore of a superconducting magnet.

REFERENCES

1 Hyunhyub Ko; Vladimir V; Tsukruk We, Liquid-Crystalline Processing of Highly Oriented Carbon Nanotube Arrays for Thin-Film Transistors, *Nano Letters*, 2006, 6 (7): 1443-1448

2 Bernadette Bensaude-Vincent, Self-Assembly, Self-Organization, Nanotechnology and Vitalism. *Nanoethics*, 2009, 3 (1):31-42

3, Candan Tamerler and Mehmet Sarikaya, Molecular biomimetics: nanotechnology and bionanotechnology using genetically engineered peptides, *Phil. Trans. R. Soc. A*, 2009, 367: 1705-1726

4 M.Le Bret, B.H. Zimm, Distribution of counterions around a cylindrical polyelectrolyte and manning's condensation theory, *Biopolymers*, 1984, 23, (287):

5 Lawrence CM, Menon S, Eilers BJ, et al., Structural and functional studies of archaeal viruses. *J. Biol. Chem.*, 2009; 284(19): 12599–12603.

6 Ki Tae Nam , Beau R. Peele, Seung-Wuk Lee, Angela M. Belcher, Genetically driven assembl of nanorings based on the M13 virus, *Nano Letters*, 2004; 4: pp23-17

7 Seung-Wuk Lee, Soo Kwan Lee, and Angela M. Belcher Virus-Based Alignment of Inorganic, Organic, and Biological Nanosized Materials, *Adv. Mater*, 2003, 15 (9):

8 Chuanbin Mao, Daniel J. Solis, Brent Iverson, Angela M. Belcher, Virus-Based Toolkit for the Directed Synthesis of Magnetic and Semiconducting Nanowires,. *Science*, 2004, 303 (5655): 213-217

9 Ki Tae Nam., Kim, Pil J. Yoo, Paula T. Hammond. Yet-Ming Chiang., Angela M. Belcher, Virus-Enabled Synthesis and Assembly of Nanowires for Lithium Ion Battery Electrodes, *Science*, 2006, 312 (12): 885-888

[10] Ki Tae Nama, Ryan Wartenaa, Pil J. Yoob, Forrest W. Liaua, Yun Jung Leea, Yet-Ming Chianga, Paula T. Hammondb, and Angela M. Belchera, Stamped microbattery electrodes based on self-assembled M13 viruses, *PNAS*, 2008, 105 (45): 17227–17231.

11 Jodie L. Lutkenhaus and Paula T. Hammond, Electrochemically enabled polyelectrolyte multilayer devices: from fuel cells to sensors, *Soft Matter*, 2007, 3: 804–816

12 Pil J. Yoo, Ki Tae Nam, Angela M. Belcher, and Paula T. Hammond, Solvent-Assisted Patterning of Polyelectrolyte Multilayers and Selective Deposition of Virus Assemblies, *Nano Letters*, 2008, 8 (4): 1081-1089.

13; Shuang Zhang, Fabrication of novel biomaterials through molecular self-assembly, *Nature Biothecnology*, 2003, 21 (10): 1171-1178.

14 Olli Ikkala and Gerrit ten Brinke, Functional Materials Based on Self-Assembly of Polymeric Supramolecules, *Science*, 2002, 295 (5564): 2407-2409

15, Nadrian C. Seeman, Angela M. Belcher, Emulating biology: Building nanostructures from the bottom up, PNAS, 2002, 99 (2): 6451–6455

16 Hammond PT, Belcher A, Park J Spontaneous assembly of viruses on multilayered polymer surfaces, *Nature Materials*, 2006 (5): 234-239

17 Vijayanathan, V.; Thomas, T.; Thomas, T. DNA Nanoparticles and Development of DNA Delivery Vehicles for Gene Therapy, *J. Biochemistry,* 2002, 41, 14085

18,Thomas, T. Polyamines in cell growth and cell death: molecular mechanisms and therapeutic applications, *J. Cell. Mol. Life Sci*., 2001, 58, 244.

19 Tang and Janmey, 1996; Tang et al., 1996, 1997, Guáqueta, C. et al, The effect of Salt on Self-Assembles Actin-Lysozyme Complexes, *Biophysical Journal*, 2006, 90, 4630-4638

20 Sanders LK, Xian W. Wong GC (2007 Control of electrostatic interactions between F-Actin and genetically modified Lysozyme in aqueous media, *PNAS*, 104 (41): 15994-15999

21 . Thomas E. Angelini, Ramin Golestanian, Robert H. Coridan, John C. Butler, Alexandre Beraud, Michael Krisch, Harald Sinn¶, Kenneth S. Schweizer, and Gerard C. L. Wong, Counterions between charged polymers exhibit liquid-like organization and dynamics, *PNAS*, 2006, 103 (21): 7962–7967.

22 Structure Lori K. Sanders, Camilo Gua´queta, Thomas E. Angelini, Jae-Wook Lee, Scott C. Slimmer, Erik Luijten and Gerard C. L. Wong]. and Stability of Self-Assembled Actin-Lysozyme Complexes in SaltyWater, *Physical Review Letters*, 2005, 95 (108302)

23 Physical Chin Li Cheung, Sung-Wook Chung, Anju Chatterji, Tianwei Lin, John E. Johnson, Saphon Hok, Julie Perkins, and James J. De Yoreo, Controls on Directed Virus Assembly at Nanoscale Chemical Templates J. *Am. Chem. Sec*., 2006, 128, 10801-10807

24 Alexander P. Lyubartsev, Jay X. Tang, Paul A. Janmey, and Lars Nordenskiöld, Electrostatically Induced Polyelectrolyte Association of Rodlike Virus Particles, *Physical Review Letter*, 1998, 24: 5465 – 5468

25 Seung-Wuk Lee and Angela M. Belcher, Virus-Based Fabrication of Micro- and Nanofibers using Electrospinning, *Nano letters*, 2004, 4 (3): 387-390

26 Seung-Wuk Lee, Bryant M. Wood Angela M. Belcher, Chiral smectic C Structrures of Virus-Based Films, *Langmuir*, 2003, 19: 1592-1598

27 Source from physic department of California polytechnic state university: http://www.calpoly.edu/~phys/

28 Jonathan Wood, Viruses rise to the surface / DNA attached to single pores for biodetection, *Resarch News*, 2006, 9 (4) pag. 15.

29 Seung-Wuk Lee, Chuanbin Mao, Christine E. Flynn, Angela M. Belcher, Ordering of Quantum Dots Using Genetically Engineered Viruses, *Science*, 2002, 296 (892)

30, Marcel Ottiger, Nico Tjandra, Ad Bax, Magnetic Field Dependent Amide 15N Chemical Shifts in a Protein-DNA Complex Resulting from Magnetic Ordering in Solution, *J. Am. Chem. Soc*. 1997, 119: 9825-9830

31 Mao C.; Solis D.J.; Reiss B.D.; Kottmann S.T. Sweeney RY, Hayhurst A, Georgiou G, Iverson B, Belcher AM. Virus-based toolkit for the directed synthesis of magnetic and semiconducting nanowires, *Science*. 2004, 303(5655): 213-217.

32 Nam K.T.; Kim D.W.; Yoo P.J.; Chiang C.Y. Meethong N, Hammond PT, Chiang YM, Belcher AM. Virus-enabled synthesis and assembly of nanowires for lithium ion battery electrodes. *Science*. 2006, 312(5775): 885-888.

33. Onsager, L. Ann. (N.Y.) The Effects of Shape on the Interaction of Colloidal Particles, *Acad. Sci*., 51(4): 627-659.

34. Z. Dogic, K. Purdy, E. Grelet, M. Adams, and S. Fraden. Isotropic-Nematic phase transition in suspensions of filamentous virus and the neutral polymer Dextran, *Phys. Rev*. 2004, 69: 51702.

35 Zweckstetter M, Hummer G, Bax A. Prediction of charge-induced molecular alignment of biomolecules dissolved in dilute liquid-crystalline phases. *Biophysical J*., 2004, 86(6):3444-60

36 Z. Dogic and S. Fraden, Cholesteric Phase in Virus Suspensions, Langmuir, 2000, 16: 7820-7824.

37 Liu DJ, Day LA, Pf1 virus structure—helical coat protein and DNA with paraxial phosphates, Science, 1994, 265: 671–674.

38, Source from Labviewer software; a 3D molecular representation program using the 1PJF.pdb file.

39 Torbet J, Maret G., Fibres of highly oriented Pf1 bacteriophage produced in a strong magnetic field, *J Mol Biol*, 1979, 134(4): 843-845.

40 K. R. Purdy, S. Varga, A. Galindo, G. Jackson, and S. Fraden, Nematic Phase transitions in Mixtures of Thin and Thick Colloidal Rods, *Phys. Rev. Letters*. 2005, 94, 057801

41 Z. Dogic and S. Fraden, Complex Colloidal Suspensions, Gompper, G / Schick, M (eds.), *Soft Matter*, 2;, 1st ed., *Wiley-VCH, Weinheim,* 2006. Chap. 1: "Phase Behavior of Rod-Like Viruses and Virus–Sphere Mixtures"

42.K. R. Purdy and S. Fraden. Isotropic-cholesteric phase transition of filamentous virus suspensions as a function of rod length and charge, *Phys. Rev.*, 2004, 70, 61703.

43.Marie Adams, Zvonimir Dogic, Sarah L. Keller, and Seth Fraden. Entropically driven microphase transitions in mixtures of colloidal rods and spheres, *Nature*, 1998, 393, 349-352.

44 Gonzalez A, Nave C, Marvin DA. Pf1 filamentous bacteriophage: refinement of a molecular model by simulated annealing using 3.3 A resolution X-ray fibre diffraction data. *Acta Crystallogr D Biol Crystallogr*. 1995, 51(5): 792-804.

45 Thiriot DS, Nevzorov AA, Zagyanskiy L, Wu CH, Opella SJ. Structure of the coat protein in Pf1 bacteriophage determined by solid-state NMR spectroscopy, *J Mol Bio,*. 2004, 341(3): 869-79.

46 Tjandra N, Bax A. Direct measurement of distances and angles in biomolecules by NMR in a dilute liquid crystalline medium. *Science*. 1997, 278(5340):1111-1114.

47 Markus Zweckstetter and Ad Bax Prediction of sterically induced alignment in a dilute liquid crystalline phase: aid to protein structure determination by NMR. *J. Am. Chem. Soc.* , 122, (2000) 3791-3792

48 Caldeira, J., Figueirinhas, J. L., Santos, C., Godinho, M. H. EPR spectroscopy of protein microcrystals oriented in a liquid crystalline polymer medium. *J. Mag. Res*, 2004, 170 (I2): 213-219.

49, Strahler, Arthur; Amino acid sequences in cytochrome c proteins from different species, *Science and Earth History*, 1997. pag. 348.

50 A. Wittemann and M. Ballauff, Interaction of proteins with linear polyelectrolytes and spherical polyetrolyte brushes in aqueous solution, *Phys. Chem. Che. Phys*, 2006, 8, 5269-5275

51 Turner D.L. Evaluation of 13C and 1H Fermi contact shifts in horse cytochrome c. The origin of the anti-Curie effect. *Eur J Biochem*, 1993, 211(3), 563-568.

52 Source from (PDB:1HRC) | http://commons.wikimedia.org/wiki/File:Cytochrome_c.png] Klaus Hoffmeier, 2006-11-20.

53 Paul E. West, Introduction to Atomic Force Microscopy Theory Practice Applications 2008, charpter 1-6.

54 Piero Carlo Braga; Davide Ricci - Atomic Force Microscopy; biochemical Methods and Applications; 242; 2004

55 Peter Eaton; Paul West, Atomic Force Microscopy Oxford university press, 2010.

56 Berne, B.J.; Pecora, R. Dynamic Light Scattering; Wiley: New York, 1976

57 Zeta Potential theory-Zeta NanoSeries , charpter 16.
http://www.nbtc.cornell.edu/facilities/downloads/Zetasizer%20chapter%2016.pdf

58 Marta Sartor Dynamic Light Scattering to determine the radius of small beads in Brownian motion in a solution, University of California San Diego

59 Provencher, S. W. A constrained regularization method for inverting data represented by linear algebraic or integral equations. *Comp. Phys. Commun.*, 1982, 27: 213–227

60 () William S. Price NMR Studies of Translational Motion: Principles and Applications, *Cambridge Molecular Science*, 30 July 2009.

61 Koppel, Dennis E.. Analysis of Macromolecular Polydispersity in Intensity Correlation Spectroscopy: The Method of Cumulants. *The Journal of Chemical Physics*, 1972, 57: 4814

62 H.Löwen, E.Allahyarow, C.N.Lykos, R.Blaak, J.Dzubiella, A.Jusufi, N.Hoffmann and H.M.Harreis, *J. Phys. A : Math. Gen*, 2003, 36, 5827-5834

63 Automated Protein Characterization With The MPT-2 Autotitrator Malvern Instrument – Bioresearch online July 27, 2005. http://www.bioresearchonline.com/download.mvc/Automated-Protein-Characterization-With-The-M-0001

64 ASTM Standard D 4187-82, Zeta Potential of Colloids in Water and Waste Water, *American Society for Testing and Materials*, 1985

65 Manfred stamm - Polymer surfaces and interfaces 1º Edition - Berlin [u.a.] : Springer, c 2008.

66 Kenneth N Han Littleton, Colo. : Society for Mining, Metallurgy, and Exploration, ©2002.

67 Dongqing Li; ScienceDirect (Online service) Publisher: Oxford : Academic, 2004. Series: Interface science and technology, v. 2 http://www.nbtc.cornell.edu/facilities/downloads/Zetasizer%20chapter%2016.pdf

68 K. F. Morris and C. S. Johnson, Jr. Diffusion-Ordered Two-Dimentional Nuclear Magnetic Resonance Spectroscopy, *Progress in NMR Spectroscopy*, 1992, 19: 1-45;

69 L.M.C. Buydens et al. Assessment of techniques for DOSY NMR data processing, *Analytica Chimica Acta*, 2003, 490: 231–251

70 Rainer Kerssebaum, DOSY and Diffusion by NMR Users guide XwinNMR –Bruker, NMR Application Lab. 2002

71 Conformational; Justin L. Lorieau, Loren A. Day, and Ann E. McDermott dynamics of an intact virus: Order parameters for the coat protein of Pf1 bacteriophage, *PNAS*, 2008, 29 (105): 3010366–10371

72; Inês Gomes, Nuno C. Santos, Alexandre Quintas, Peter Eaton and Ricardo Franco Probing Surface Properties of Cytochrome c at Au Bionanoconjugates, *J. Phys. Chem. C*, 2008, 112 (42): 16340–16347

73 http://www.acdlabs.com/products/pc_admet/physchem/physchemsuite/?gclid=CJinyKH-kacCFUaIDgodcXiZcQ

74 Turner, D. L. Determination of Haem Electronic Structure in His-Met Cytochromes *c* by 13C-NMR, *Eur. J. Biochem.* 1995, 227, 829-837.

75 P.T. Callaghan, M.A. Legros, D.N. Pinder, The measurement of diffusion using deuterium pulsed field gradient nuclear magnetic resonance, *J. Chem. Phys*, 1983, 79: 6372–6381.